ISSN Application No. 21803

Indian Journal of Mechanical and Thermal Engineering

Volume No. 7

Issue No. 2

May - August 2023

ENRICHED PUBLICATIONS PVT. LTD

S-9, IInd FLOOR, MLU POCKET,
MANISH ABHINAV PLAZA-II, ABOVE FEDERAL BANK,
PLOT NO-5, SECTOR-5, DWARKA, NEW DELHI, INDIA-110075,
PHONE: - + (91)-(11)-47026006

Indian Journal of Mechanical and Thermal Engineering

Aims and Scope

Indian Journal of Mechanical and Thermal Engineering is a peer-reviewed journal for the presentation of original contributions and the exchange of knowledge and experience on the sciences of heat transfer and thermodynamics, and contribute to the literature of engineering sciences on the national and international areas but also help the development of mechanical engineering. engineers and academicians from disciplines of power plant engineering, energy engineering, building services engineering, HVAC engineering, solar engineering, Wind engineering, Nano engineering, surface engineering, thin film technologies, and computer aided engineering will be expected to benefit from this journal's conclusions.

Indian Journal of Mechanical and Thermal Engineering

Indian Journal of Mechanical and Thermal Engineering

(Volume No. 7, Issue No. 2, May - August 2023)

Contents

Steady State Thermal Approximation to Thermal Transients in Lighting Unit Design

[1] Osman Gozutok, [2] Erhan Kiliç, [3] Samet Çalişkan
[1, 2, 3]Odelo Automotive Signal Systems R&D Center, Bursa, Turkey
E- mail: [1]osman.gozutok@odelo.com.tr, [2]erhan.kilic@odelo.com.tr, [3]samet.caliskan@odelo.com.tr

A B S T R A C T

Automotive lighting technology has a rough and hard journey in the past from candle to nowadays LEDs. Having high efficacy with LEDs, luminous flux decrease is a thermal management problem that should be handled with. Minimum luminous flux requirements are determined by specific regulations and in design phase, the limits of optical design of each function in lighting unit has to be exceeded. High optical requirement results with high thermal power that has to be considered and managed in design of lighting units. Thermal management of lighting device can be handled both with thermal transients and steady state numerical approximation procedures. Thermal transient management is time consuming task and not appropriate for numerical experimentation on design of lighting device. Because of several functions that has the device to satisfy with like signal, turn indicator and tail function. Each function has to be investigated in detail through standards. Instead of thermal transients defining local power constants enable the analyst to predict transient characteristic of the function clearly. In this study defining appropriate thermal power constants for the steady state approach in order to predict thermal transient characteristic of a lighting device is investigated. Numerical results with steady state approximation are compared with test results, and appropriate power constants identified.

Keywords - Thermal Power Constants, Automotive Lighting Unit Design, Steady-State Thermal Management of Lighting Device

I. INTRODUCTION

The thermal design in automotive exterior lighting products affects reliability. Thermal management process, which include pre-design for quotation and validation tests before the serial production, is long term work. Several tests and analyses are performed at all design stages. Thermal expectation from design criteria is to make appropriate selection of material which has effects on cost, manufacturability and lifetime [1-3].

The process starts with determining thermal powers on each component, and making initial calculations for the PCBs' dimensions. Initial power estimations are defined through the electronic and the optic requisites. Options of thermal management will enable the analyst to decide the cooling strategy. Passive cooling on the PCBs is directly related with surface area, after determining the power of components. If the allocated lighting space does not dissipate heat generated to keep the components safe enough, active cooling systems are considered [4, 5]. Thermal criteria is case sensitive depending on the technology utilized in lighting. Halogen or LEDs, the light source defines the requirements from the thermal management. Even though, the plastic parts get more warmed with halogens, Vicat

softening and heat deflection temperatures of the plastics are considered in design phase for both. Headlamp and rear combination lamps have different tasks to perform. Each task is called functions of lighting unitconsidered in design phase. If headlamp and module is considered, functions are Low Beam, High Beam, Signal and Cornering. If LED is the light source, extra numerical experiments run to predict luminous flux degradation, which is caused by junction temperature of LEDs, on each functions. The degradation of LED light source, is identified as a drop in light intensity of the lighting unit and is important because of optical necessity to satisfy the regulated light pattern. Thermal transient analysis approximation to predict the degradation performance of the lighting unit is the most appropriate method for numerical experimentation. However, it is difficult and time consuming task, especially in design phase of lighting device there are several design updates and changes to be handled with. This makes thermal transient numerical solution procedure inappropriate in design phase. Instead less costly and faster numerical approximations are essential. That is the case in this study to take place, to identify suitable thermal power constants to capture thermal transient characteristics of lighting unit and to enable analyst to predict accurate thermal management of the lighting device.

In design phase, thermal simulations and the prototype tests are the main tools in decision making. In numerical experimentations, fluid and thermal simulations provide high accuracy results and, also give the chance to try-out various options to construct optimum design before the prototype tests installed and production facilities started [5].

Dynamic lighting function is not steady state lighting- on. Some function flashing, some function periodically turns On and Off. This leads difficulty of prediction of solder point temperature of hot-spot locations on the PCB.Generally thermal approaches for unsteady, which can be assumed steady-state after multiply by suitable constant. However, this formulation not gives you, values at 30th minute, to predict the degradation of LED's utilized in the lighting device. Temperature changes during the period of time, transient solutions should be adopted [6-9].

Steady state solution approximates the value that there is no change depending on time is the case. In a lighting scenario, every function of the lighting unit is active periodically, permanently or flashing. Understanding the effects of function modes are critical to get accurate results compared with test.

Identifying thermal management results of the product enables the analyst to evaluate the performance of the lighting unit. Approximating the thermal management of a lighting device with steady state numerical solutions reduces the time needed for the solution and eases the solution procedure. However, steady state solution approximation needs power constants to be identified that will take place in the thermal management of lighting device.

II. STEADY-STATE SOLUTION SCENARIO CONSTANTS

All test were performed 23°C ambient temperature conditions. Tail, Stop, Signal and Reverse function were reviewed. Each function has different scenario and different power constant to be adopted. Temperature of LED's and some control component were measured.

Lighting Function Scenario Results

Tail function is permanently lighting-ON. Tail semiconductors' temperatures were reached %92 values before the 30th minute. It can be predicted that %97 values are at the 60th minute and %100 values after the 90th minute.

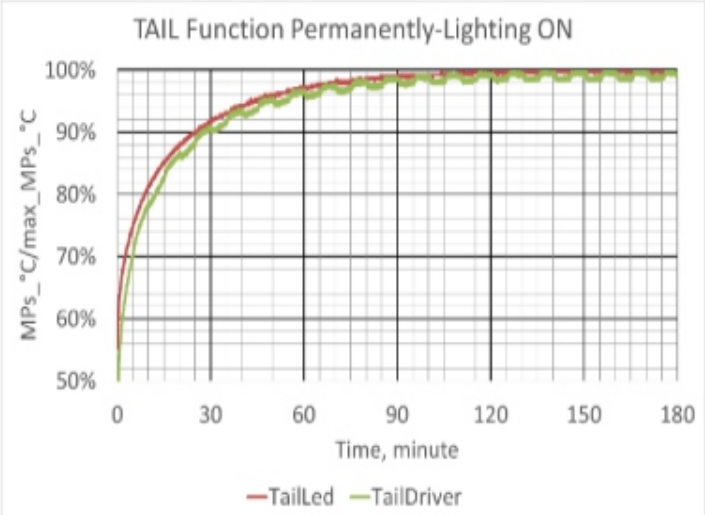

Fig.1. Temperature measurements for tail function permanently lighting on during 180 minutes

Stop function period is 20 seconds ON and 5 seconds OFF. Stop semiconductors' temperatures were reached %83 values before the 30th minute. It can be predicted from Fig. 2 that %97 values are at the 60th minute and %100 values after the 90th minute.

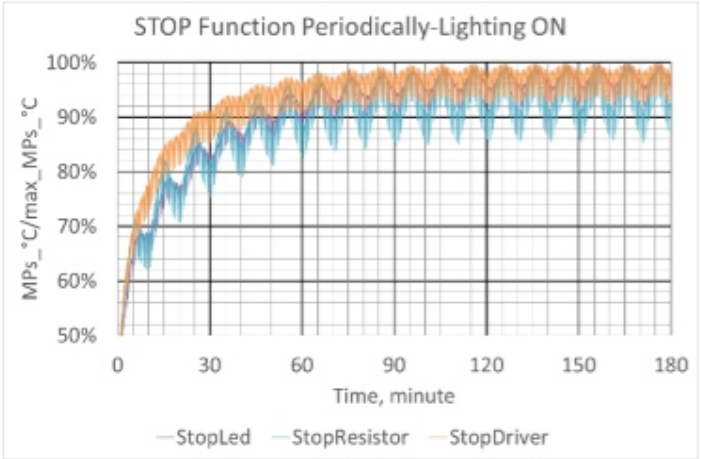

Fig.2. Temperature measurements for stop function periodically lighting on during 180 minutes

Signal function is continuously flashing. Signal semiconductors' temperatures were reached %83 values before the 30th minute. It can be predicted from Fig. 3 that %97 values are at the 60th minute and %100 values after the 90th minute.

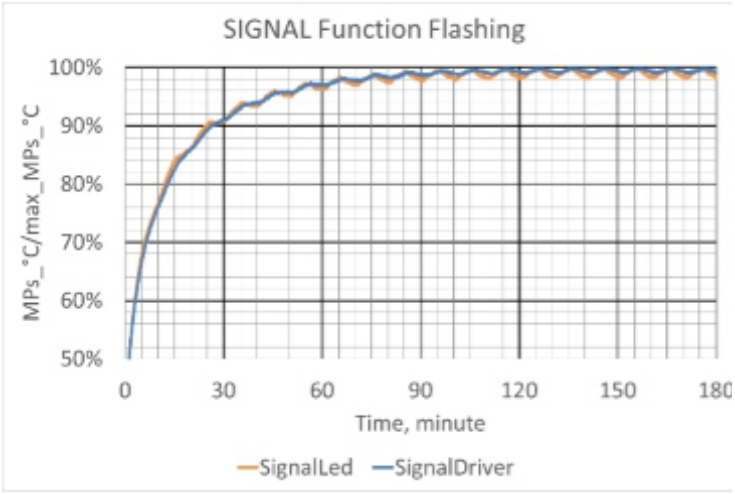

Fig.3. Temperature measurements for signal function flashing lighting on during 180 minutes

Reverse function period is 5 minutes ON and 5 minutes OFF. Reverse semiconductors' temperatures were reached %94 values before the 30th minute. It can be predicted from Fig. 4 that %99 values are at the 60th minute and %100 values after the 90th minute.

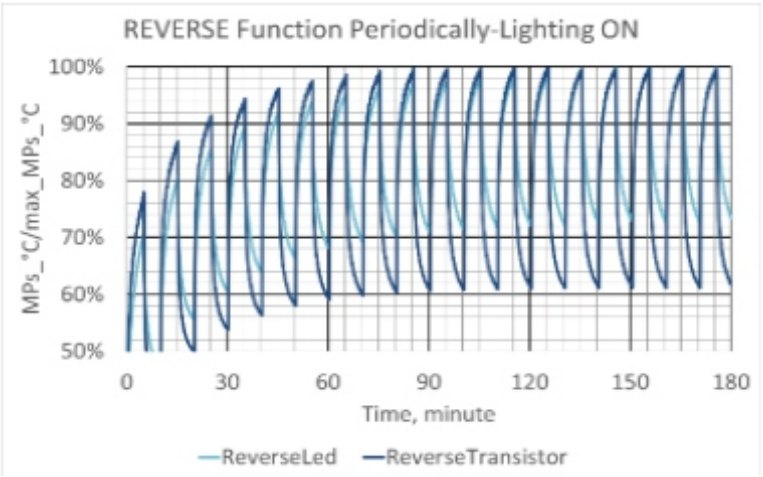

Fig.4. Temperature measurements for reverse function periodically lighting on during 180 minutes

Evaluation of Scenario Constants

In the evaluation of the scenario constants or power constants, each function one-by-one is activated permanently during 90 minutes. Meaning that no scenario is identified.

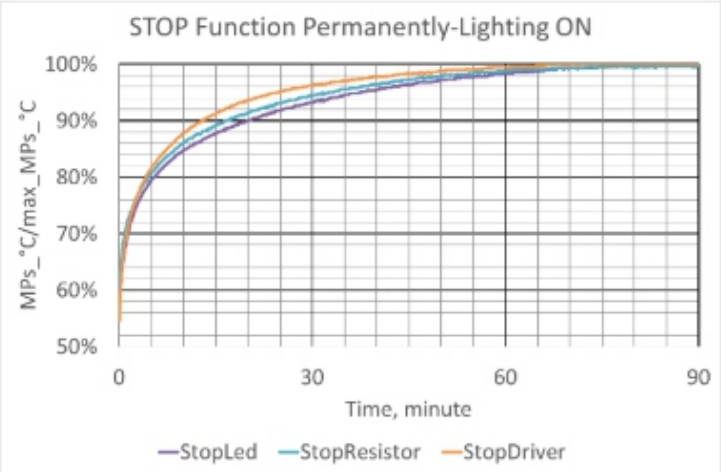

Fig.5. Temperature measurements for stop function permanently lighting on during 90 minutes

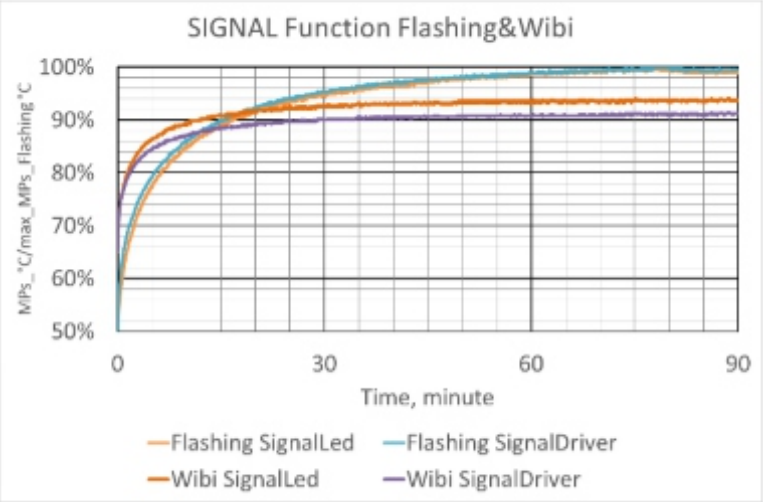

Fig.6. Temperature measurements for signal function flashing/wibi lighting on during 90 minutes

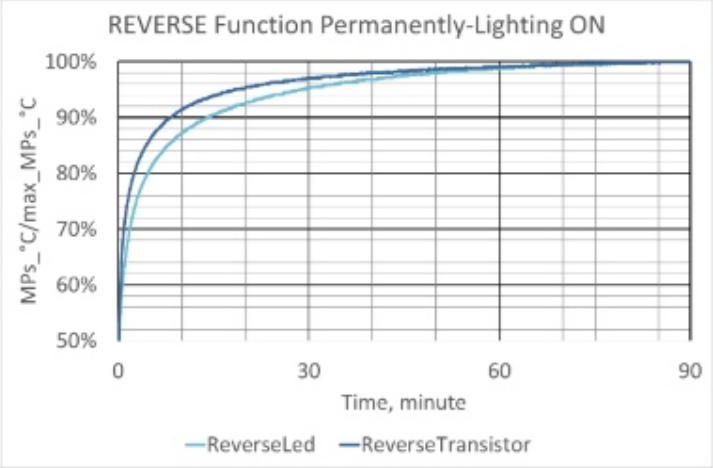

Fig.7. Temperature measurements for reverse function permanently lighting on during 90 minutes

Results predicted in Fig. 5 to Fig. 7 identifies the thermal characteristic of each function in 90 minutes period. That is further be utilized in predicting scenario or power constants in comparison with the thermal transients of the test of each function in the lighting unit.

III. RESULTS AND DISCUSSION

3.1. Scenario Constants(Power Constants)

In a typical automotive signal lighting scenario all the functions can be lighting-ON same time or subsequently. All these periodical values were applied for related functions and starting the lighting-ON at lighting unit. Case with scenario and Case without scenario were overlapped and determined the scenario or power constant for that function. The results of the study show that power constants vary with the scenario. These results can be employed in steady state thermal analysis.

Stop function scenario constant are evaluated 0.84 for LED, 0.87 for resistor component and 0.88 for driver component.

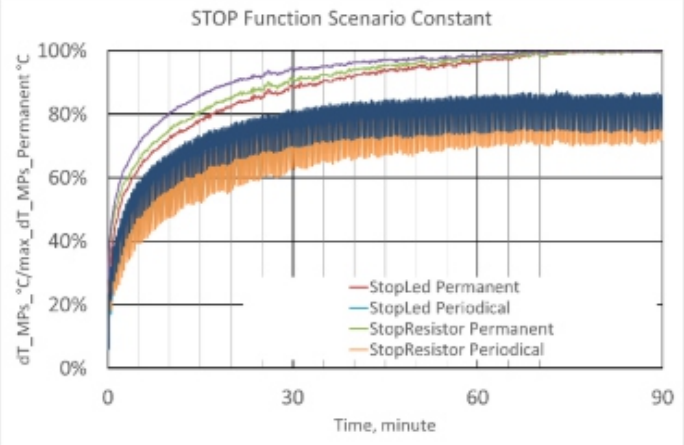

Fig.8. Scenario constants calculations for stop function during 90 minutes

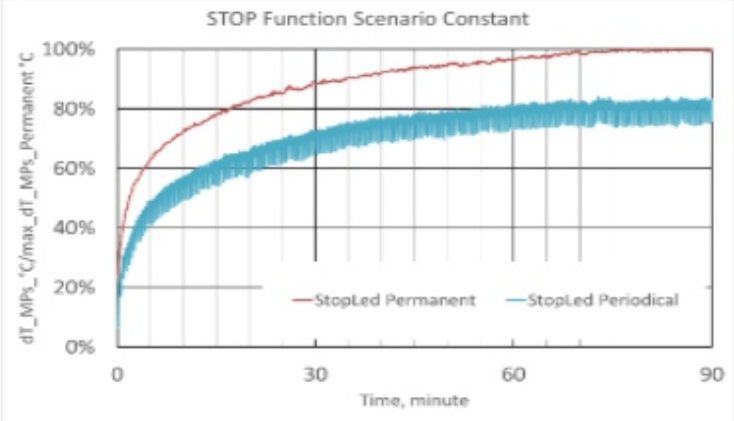

Fig.9. Scenario constants calculations for stop function LED during 90 minutes

Reverse function scenario constants are evaluated 0.82 for LED and 0.88 for Transistor component.

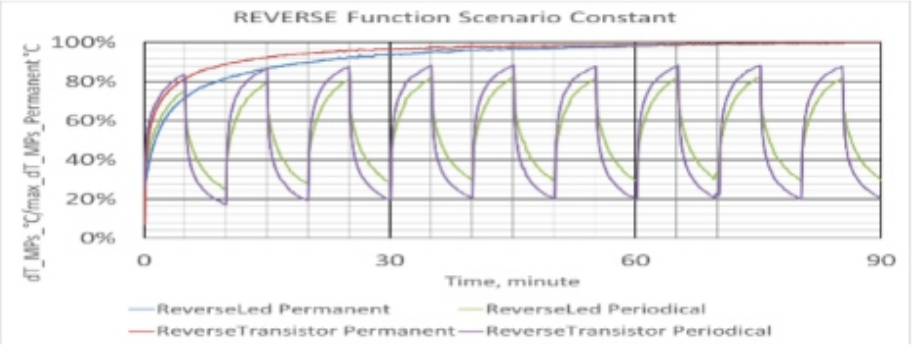

Fig.10. Scenario constants calculations for reverse function during 90 minutes

Signal function with flashing scenario constants are evaluated 0.64 for LED and 0.64 for Driver component. Signal function with Wibi scenario constants are evaluated 0.56 for LED and 0.53 for Driver component.

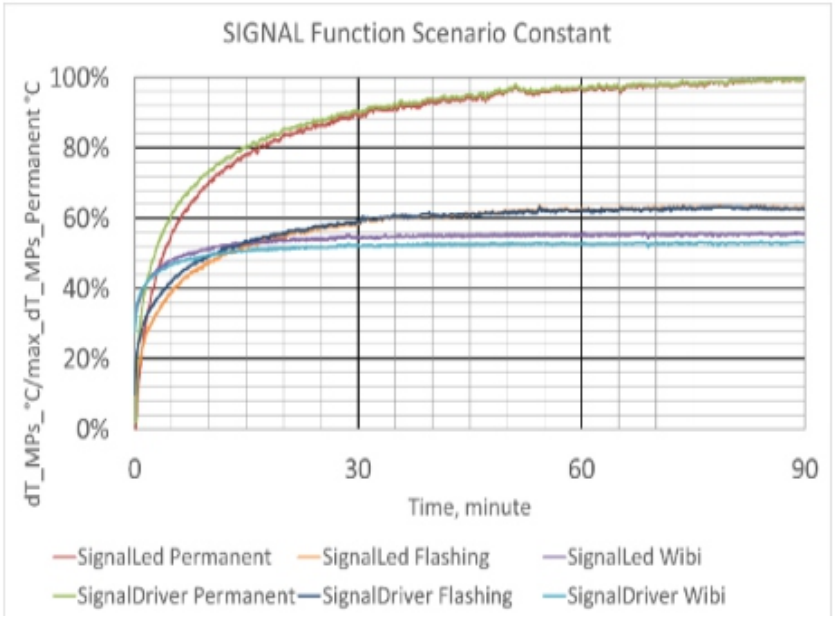

Fig.11. Scenario constants calculations for signal function during 90 minutes

		Scenario Constants			
		LED	Driver	Resistor	Transistor
Tail	Continously ON	1	1	1	1
Stop	20s ON/5s OFF	0,84	0,88	0,87	-
Reverse	5m ON/5m OFF	0,82	-	-	0,88
Signal_Flashing	Continously Flashing	0,64	0,64	-	-
Signal Wibi	Continously Wibi	0,56	0,53	-	-

Table 1: Scenario constants for signal lambs

Predicted steady state thermal simulation with the scenario or power constants depicted through Fig. 12 and Fig. 15. In steady state thermal management power of each component is defined with the appropriate scenario constant defined through function tests.

Fig.12. Simulation results for Tail LEDs

Fig.13. Simulation results for Stop LEDs

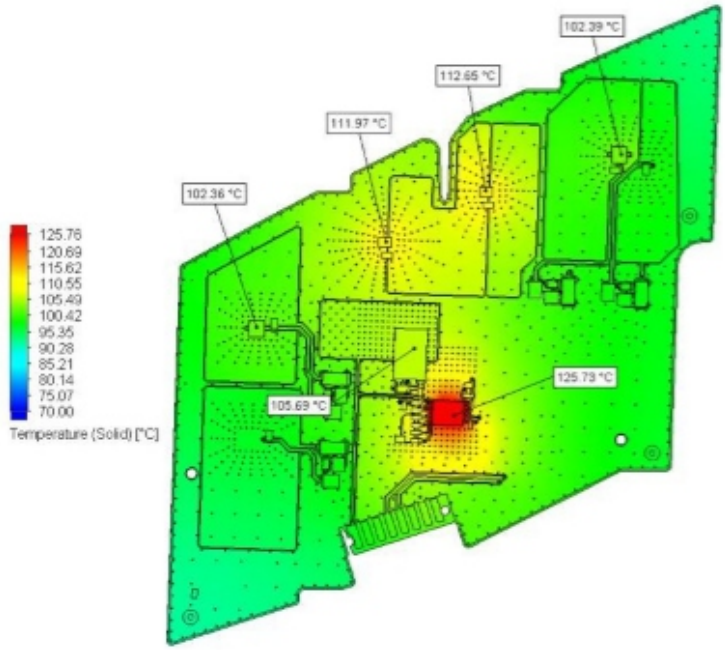

Fig.14. Simulation results for Reverse LEDs

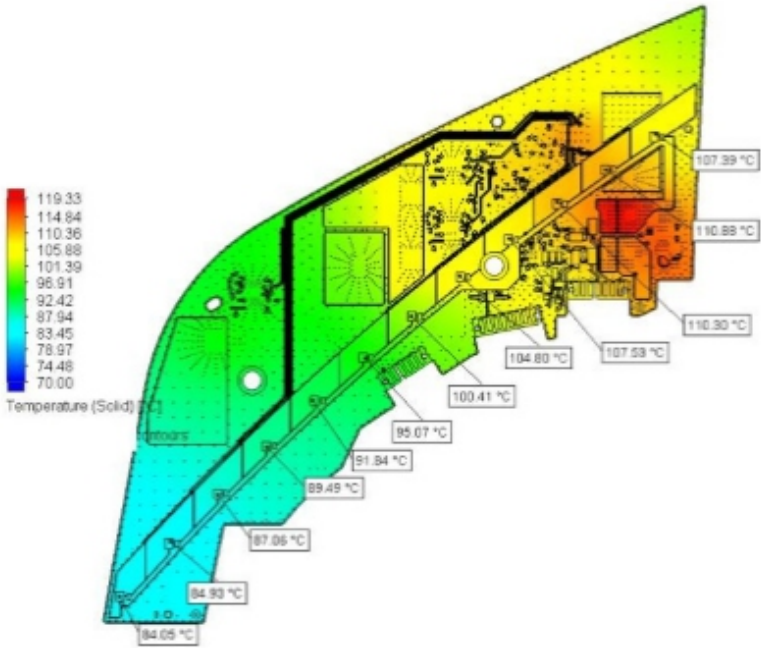

Fig.15. Simulation results for Signal LED

Temperature distribution on each component in the steady state thermal management has a very good agreement with the results obtained in tests. Test environment includes transient effects that comes from active cooling and heating system that has to be set to a certain environment temperature in the chamber. However, in steady state thermal management process these effects are all approximated through thermal scenario or power constants. Predicted approximation presented in this study is a proper alternative way of predicting the thermal transient effects employing scenario or power constants approach.

Measurepoint	Measured Function LED	Climate Chamber Test Results at 70°C			Simulation Results at 70°C with Scenario Constants	Error	
		Sample 1	Sample 2	Average	Tmax, °C	dT, °C	%
MP01	TAIL	73 °C	74 °C	73 °C	81,88	8,88	12%
MP02	STOP	92 °C	93 °C	93 °C	97,62	4,62	5%
MP03	REVERSE	95 °C	97 °C	96 °C	102,39	6,39	7%
MP04	SIGNAL	106 °C	105 °C	105 °C	110,88	5,88	6%

Table 2: Comparison of Steady State Simulation results with Scenario constants for Lighting unit functions and Tests.

IV. CONCLUSION

In this study,

An approach to identify thermal scenario constants or power constants presented. Identified scenario constants are defined and employed in thermal steady state approach.

Thermal transient effects are captured employing scenario constants in steady state thermal analysis approach. Results are in very good agreement with test results obtained in thermal chamber.

REFERENCE

[1] Hamm M., and Huhn W., (2008) SAE Technical Paper Series (2008-01-0337), Design claims and technical solution steps generating the world first full LED headlamp

[2] Ott H., and Nylander J., (2002) SAE Technical Paper Series (2002-01-0383), Ultra-thin automotive lamps (8-12mm) using special SMT LEDs and special optics.

[3] DrivingVisionNews.com, Vehicle lighting in Japan technics, Automakers, Tier1 and Tier2, (2018)

[4] Mauney C., Texas Instruments, Thermal considerations for surface mount layouts

[5] Kikuchi K., Hamashima Y., and Kobayashi Y., (2005), SAE Technical Paper Series (2005-01-0864), An approach to predicting LED junction temperatures with fluid and thermal analysis

[6] Mentor®, 2018, FloEFD for CATIA V5 technical reference, software version 17.

[7] Osram, OSLON® Black Flat, technical datasheet KW H3L531.TE, http://www.osram.com, 01 October 2018.

[8] Ansari A., Ince W., and Sayers M., (2007), SAE Technical Paper Series (2007-01-1037), Towards development of thermal standards for the design of LED lamps.

[9] Donahoe D. N., (2009) IEEE, Thermal aspects of LED automotive headlights

Thermo Gravimetric Study on Thermal and Combustion Characteristics of Thai Lignite, Rice Husk, and their Mixtures

[1] Rajita Jirapraditkul, [2] Saran Chinwanno, [3]Nichaporn Sararak, [4]Vladimiri. Kuprianov

[1]School of Manufacturing Systems and Mechanical Engineering, Sirindhorn International Institute of Technology, Thammasat University, P.O. Box 22, Thammasat Rangsit Post Office, PathumThani 12121, Thailand.

E-mail: [1]aomifs.a@hotmail.com, [2]saran252623@hotmail.com, [3]nichaporn.sar@gmail.com, [4]ivlaanov@siit.tu.ac.th

A B S T R A C T

The combustion behavior and characteristics of Thai lignite, rice husk, and their blends in different proportions were investigated in a thermogravimetric analyzer. In each thermogravimetric test, a 15-mg sample (lignite/biomass/blend) was heated in the analyzer furnace from 30 °C to 900 °C, using dry air as a furnace gas. Three test series, aimed at studying the effects of (i) lignite and biomass proportions in the blend, (ii) heating rate, and (iii) flow rate of the furnace gas on the TG/DTG profiles (characterizing the decomposition behavior of the samples), were performed. The characteristic temperatures were obtained from the analysis of TG/DTG curves for the selected fuel options and operating conditions. The kinetic parameters were determined for a model predicting the time-related decomposition of lignite/biomass blends for different operating conditions, using the Coats-Redfern method. The experimental results revealed excellent combustion properties of both selected fuels. However, rice husk exhibited higher thermal and combustion reactivity, compared to Thai lignite, and therefore can be used as a secondary/reburn fuel in fuel-staged co-firing systems, leading to lower environmental impacts.

Keywords - Thai lignite, Rice husk, Thermogravimetric analysis, Operating conditions, Kinetic parameters.

I. INTRODUCTION

In Thailand, low-rank Thai lignite has been used for many years as one of the major fossil fuels for power generation. The Mae Moh power plant with an installation capacity of 2455 MW is the only lignite- based utility in this country [1]. Because of the low quality of Thai lignite and elevated contents of sulphur, nitrogen, and ash in the fuel, the power plant is a strong contributor to air pollution in Northern Thailand. Co-firing of coal with biomass is reported to be an effective tool for the improvement of environmental characteristics (reduction of harmful emissions) and thermal efficiency of boiler units, as compared to firing coal on its own, mainly due to substantially lower proportions of sulphur, nitrogen, and mineral matter in biomass [2]. The use of fuel staging and re-burning during co-firing of coal and biomass results in a reduction of NOx emissions, as compared to burning coal alone (oraspre-mixed with biomass) in a single combustion system [2,3].However, the combustion reactivity of biomass (containing hemi cellulose, cellulose, and lignin) is basically higher than that of coal [4,5]. This difference in fuel reactivity may cause some problems, such as fuels segregation and deterioration in combustion efficiency, when co-firing coal and biomass in systems (e.g., pulverized coal-fired

boilers and fluidized-bed combustors) using fuel staging and reburning[3]. With a great availability and energy potential of 93 PJ per year, domestic rice husk is considered to be an important biomass energy resource in Thailand. Previous research studies have shown an effectiveness of this biomass as a secondary/reburn fuel for NOx reduction in fluidized- bed systems co-fired with two different fuels [3]. Thermo gravimetric analysis (TGA) has been used to investigate and compare the thermal and combustion reactivity of individual fossil and biomass fuels, and fuel blends including coal–biomass mixtures [6– 8].Thermo gravimetric (TG) and derivative thermo gravimetric (DTG) curves, the major output of a TGA study, are basically obtained to characterize the de- volatilization and combustion behavior of selected fuels/blends and the specific temperatures. Results from the TG/DTG tests provide an important data for determining some kinetic characteristics to build up a semi-empirical model describing the time-related decomposition of a fuel/blend [6]. This work was aimed at studying the degradation behavior and thermal/combustion characteristics of Thai lignite, rice husk and their blends in different proportions, with an objective to assess the effectsof operating conditions on those characteristics and to compare thermal/combustion reactivity between the selected fuel options. The specific (ignition, peak, and burnout) temperatures, as well as kinetic modeling of fuel decomposition, were the focus of this work.

Fuel	Ultimate analysis (wt.%, on as-received basis)					Proximate analysis (wt.%, on as-received basis)				LHV (MJ/kg)
	C	H	N	O	S	W	VM	FC	A	
Lignite	32.50	2.44	1.28	17.47	3.66	12.26	38.64	18.71	30.39	11.68
Rice husk	36.60	4.69	0.31	34.01	0.33	8.87	60.96	14.98	15.19	13.65

Table 1: Ultimate and proximate analyses, and the lower heating value (LHV of Thai lignite and rice husk.

II. FUEL PROPERTIES

Table 1showsthe properties of fuels, the ultimate and proximate analyses and the lower hating value of Thai lignite (L) and rice husk (RH).Both fuels show a high amount of volatile matter, indicating their high combustion reactivity. However, the volatile matter in the biomass was greater than that in lignite, while the fixed carbon showed an opposite trend. Prior to the TGA tests, lignite was kept in air at the ambient temperature for a while. Therefore, the fuel moisture was not as high as that “fresh” mined lignite. For this reason, the LHVs of the two fuels were rather similar, LHV = 11.68 MJ/kg for lignite and LHV = 13.65 MJ/kg for rice husk. Taking into account greater fuel- N, fuel-S, and ash contents in lignite, as compared to rice husk, one can expect an improvement of environmental characteristics of a combustion system after switching from firing lignite to co-firing lignite with the selected biomass.

III. TG/DTG ANALYSIS: A SYSTEM AND OPERATING CONDITIONS

A "Mettler Toledo" TGA/DSC1 thermo gravimetric system (analyzer) was employed to obtain the thermo gravimetric characteristics (TG and DTG curves) for the selected fuel options. Dry air was used as the furnace environment in this analyzer, which was supplied into the analyzer furnace. To exclude the effects of the fuel particle size on the above characteristics [9], both biomasses were ground and sieved prior to testing, to ensure fine particle sizes (less than 200 μm).Fig. 1 depicts the original lignite ø èparticles and those (like powder) after the grinding process, whereas Fig. 2 shows the original husks in comparison with the ground biomass. Five lignite– biomass blends were then preparedin different weight (mass) proportions: 100% L, (75% L + 25% RH), (50% L + 50% RH), (25% L + 75% RH), and 100% RH. During each TGA test, a 15-mg biomass/blend sample was heated in each TGA tests from 30 °C to 900 °C.

Three experimental series were performed in this work. At the first stage, the TGA tests were conducted for the above fuel options at a fixed furnace heating rate and constant flow rate of the dry air. The second test series was performed for the fixed (typical) proportion of the fuels (75% L + 25% RH)at the constant flow rate of the furnace gas (dry air), for four different furnace heating rates (10, 20, 30, and 40 °C/min). The third test series was performed for a variable flow rate of the furnace gas (20, 30, 40, and 50 ml/min) using the (75% L + 25% RH) mixture, when keeping the furnace heating rate constant. Note that the TGA test for fixed operating conditions was performed several times for repeatability. Some thermo gravimetric characteristics, such as ignition temperature (T_{ign}), peak temperatures (Tp,1 and $T_{p,2}$), and burnout temperature (T_b), were determined from the TG/DTG curves [10] and then compared between the fuel options.

IV. KINETIC STUDY

Kinetic modeling was studied using Coats-Redfern method [11] to determine the characteristics of biomasses and their mixtures in thermogravimetric tests. Ignoring the process of biomass dehydration, the biomass decomposition rate (α) can be defined as follows:

$$\alpha = \frac{w_0 - w_\tau}{w_0 - w_f} \qquad (1)$$

where w_0, w_f, and w_t are the initial, final and current (at time t) weights of the biomass sample.

Kinetic equation represented in term of an "n-th" order model and describe biomasses decomposition with respect to time as:

$$\frac{d\alpha}{d\tau} = A\exp\left(-\frac{E}{RT}\right)(1-\alpha)^n \qquad (2)$$

where A is the pre-exponential factor, E is the activation energy, R is the universal gas constant, and T is time-related (current) temperature.

Recall that the heating rate of the gas is $\beta = T/\tau$ and the experiment conducts at constant heating rate (β = constant), Eq. (2) can be rewritten in the form:

$$\frac{d\alpha}{(1-\alpha)^n} = \frac{A}{\beta} \exp\left(-\frac{E}{RT}\right) dT \qquad (3)$$

Taking into account the major assumption of the Coats-Redfern method (i.e., $2RT/E << 1$), and assuming that the value of E is unchanged over a selected temperature range, Eq. (3) after its integration yields as:

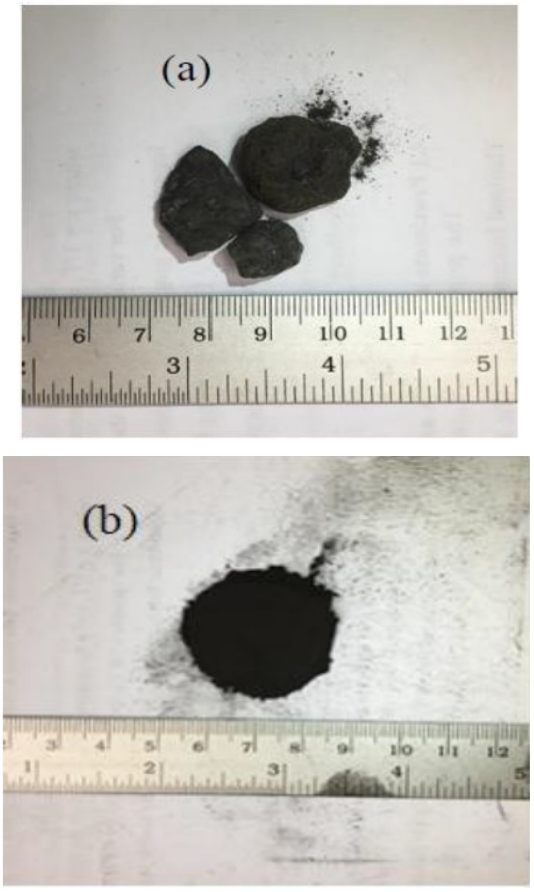

Figure 1: Thai lignite particles: (a) original and (b) ground.

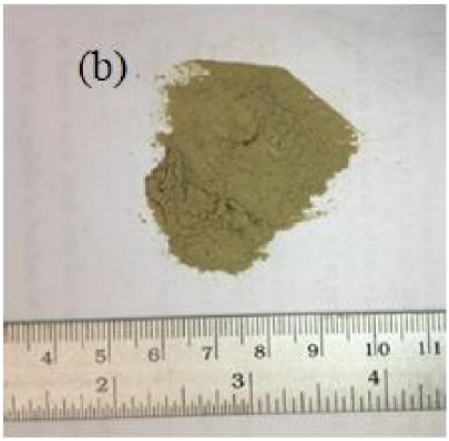

Figure 2: Rice husk particles: (a) original and (b) ground.

$$\text{for } n = 1: \quad -\ln\left[-\frac{\ln(1-\alpha)}{T^2}\right] = -\ln\left[\frac{AR}{\beta E}\right] + \frac{E}{RT} \qquad (4)$$

$$\text{for } n \neq 1: \quad \ln\left[\frac{1-(1-\alpha)^{1-n}}{T^2(1-n)}\right] = -\ln\left[\frac{AR}{\beta E}\right] + \frac{E}{RT} \qquad (5)$$

The left-hand side of Eq. (4) and Eq. (5), can be designated as y. With the properly selected n, the experimental data from a thermogravimetric test can be fitted by a first-order curve:

$$y = a + bx \qquad (6)$$

where x = 1/T, and a designates the first term on the right-hand side of Eq. (4) and Eq. (5).

For variable x (or T), the curve y = f(x) for the selected n can be then plotted on a semi- logarithmicgraph to quantify the kinetic constants: E (by using the fit slope b) and A (from the expression for a).

V. THERMOGRAVIMETRIC ANALYSIS OF THE ORIGINAL FUELS

Fig. 3 shows the TG/DTG curves of lignite and rice husk tested individually at the heating rate of 20°C/min, when using dry air as the furnace gas with the flow rate of 30 ml/min.From Fig. 3, the TG curves of both fuels showed rather similar trends, apparently exhibiting sequent stages (temperature regions) associated with:(1) sample dewatering, (2) volatilization of the fuels, accompanied by volatile oxidation by the dry air, and (3) oxidation of fuelchars.

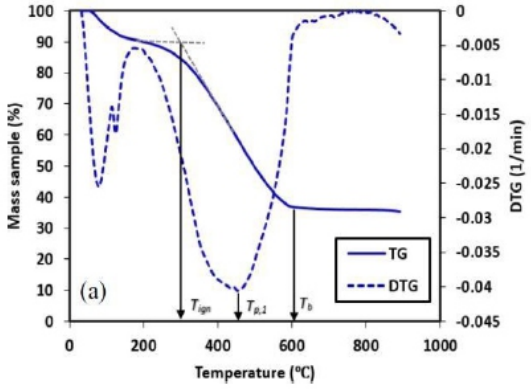

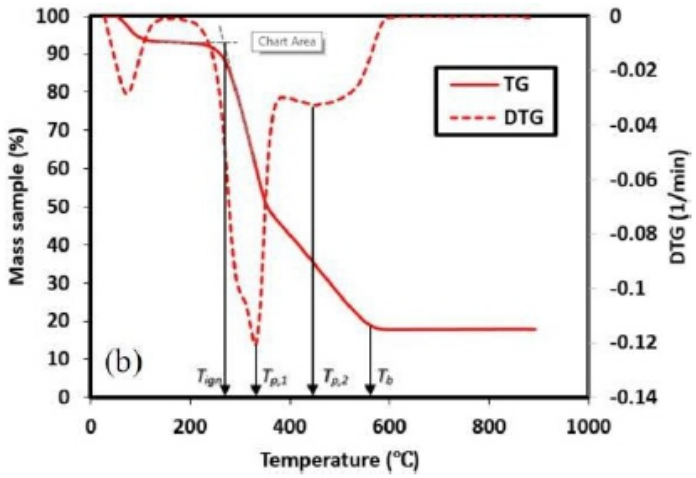

Figure 3: TG and DTG curves of (a) lignite and (b) rice huskdecomposed in dry air of 30 ml/min at the heating rate of 20 °C/min.

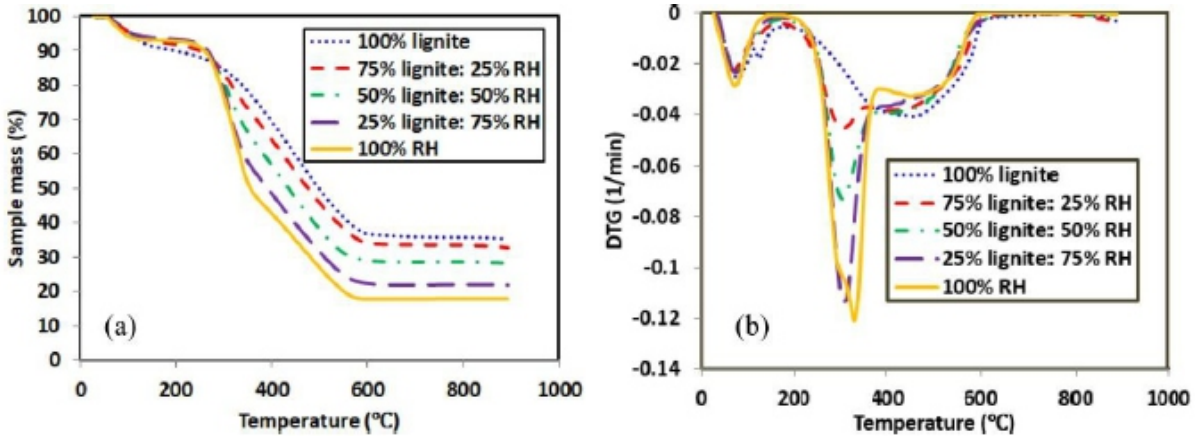

Figure 4: Effects of the proportions of Thai lignite and rice huskon (a) TG and (b) DTG curves.

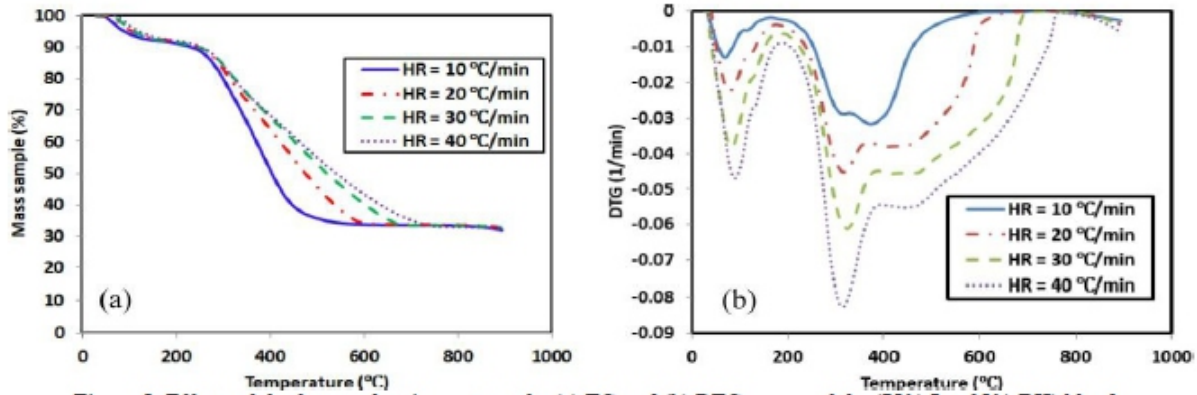

Figure 5: Effects of the furnace heating rate on the (a) TG and (b) DTG curves of the (75% L + 25% RH) blend.

Figure 5: Effects of the furnace heating rate on the (a) TG and (b) DTG curves of the (75% L + 25% RH) blend.

From the DTG curves in Fig. 3, for Thai lignite decomposition, the ignition temperature (T_{ign}) was 304 °C, whereas the (first) peak temperature (Tp1) was452 °C. For rice husk, they were apparently lower:

273 °C only 331 °C, respectively. However, the ignition temperatures(T_{ign}) for the two fuels were rather close to each other: 602 °C for lignite and 566°C for rice husk. These date indicating a significant decomposition difference between coal and biomass; however, the combustion reactivity of Thai lignite was somewhat lower, compared to that of rice husk, as follows from the analysis of data in Fig. 3.

VI. EFFECTS OF FUEL PROPORTIONS IN A LIGNITE–BIOMASS MIXTURE

Fig. 4 depicts the TG and DTG curves of the fuel blends mixed in different proportions, along with those for pure lignite and rice husk, for the selected (fixed) operating conditions (as specified above).

From Fig. 4, all the TG and DTG curves of the blends were located in between the ones of pure lignite and pure rice husk. Like in Fig. 3, the TG and DTG curves of the fuel blends showed different stages (temperature regions), and the specific temperatures (T_{ign}, $T_{p,1}$, $T_{p,2}$ and T_b), listed in Table 2.From Table 2, with increasing proportion of rice husk in a blend, the decomposition rate of the mixture rapidly increased at the first peak temperature, which (as seen in Table 2) showed the trend to decrease, indicating an increasing thermal reactivity of the blend.

Note that with addition of a relatively small proportion of rice husk to pure lignite, the burnout temperature was apparently decreased, showing higher combustion reactivity, likely due to facilitation of the oxidation of the fuel blend by volatile from biomass. However, Tbwas nearly constant for all the tested blend at a level close to the burnout temperature of pure rice husk. Unlike$T_{p,1}$, $T_{p,2}$ showed rather weak effects of the fuel proportions.

Sample	Temperatures (°C)			
	Tign	Tp,1	Tp,2	T_b
100%Thai lignite	304	452	-	602
75%Thai lignite + 25% rice husk	266	314	417	551
50% Thai lignite + 50% rice husk	265	304	417	550
25% Thai lignite + 75% rice husk	275	313	426	558
100% rice husk	273	331	452	566

Table 2:Characteristic temperatures of lignite–biomassmixtures decomposed at the heating rate of 20 °C/min and furnace gas (dry air) flow rate of 30 ml/min.

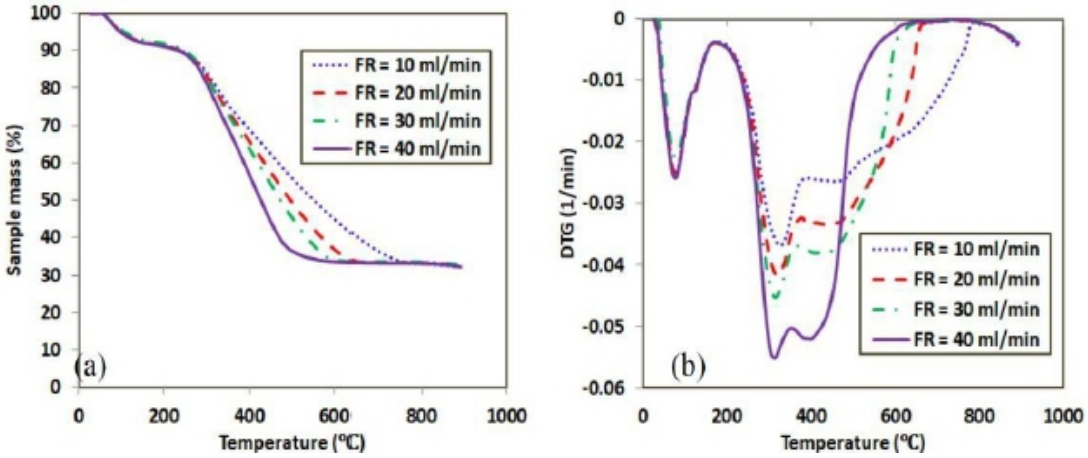

Figure 6: Effects of furnace gas (dry air) flow rate on the (a) TG and (b) DTG curves of the (75% L + 25% RH) blend.

VII. EFFECTS OF THE FURNACE HEATING RATE

Figure 5 shows the TG/ DTG profiles of Thai lignite and rice husk tested at different heating rates and constant furnace gas flow rate of 30 ml/min.

The maximum peak (combustion rate) and the yield of volatile matter increases as heating rate getting higher. Since the process has less time available for tar cracking and consequently the more tar and the less methane are produced, the heat transfer is not as effective as they were at lower heating rates. The burnout temperatures shift to higher temperature.

VIII. EFFECTS OF THE FURNACE GAS FLOW RATE

Figure 6 depicts TG/DTG profiles of the samples tested at different furnace gas flow rates and constant heating rate of 20 /min. The furnace gas flow rates are not affect the temperature range in moisture removal and ignition temperature.

At the lower furnace gas flow rates, the fuel decomposition was slower shifting the burnout temperatures shift to a higher level. With increasing the furnace gas flow rate, the char oxidation was found to be faster.

IX. KINETIC PARAMETERS

The kinetic analysis was performed using the semi- empirical Coats-Redfern method. This approach enables to obtain the decomposition (combustion) kinetics modeling of Thai lignite, rice husk and their mixtures.

The kinetic parameters such as the activation energy (E), pre-exponential factor (A) and reaction order (n) were obtained from the relationship between logarithm function and inverse of temperature (1/T). The plotted graph will give a straight line with slope E/R, y-intersect AR/βE and high coefficient value of regression coefficient (R2) mainly above 90%. The kinetics modeling was derived into three conditions; different proportion, different furnace heating rates and different furnace gas flow rates.

Table 3 shows that the addition of rice husk to pure Thai lignite increases the activation energy (E) and pre-exponential factor (A) at the lower temperatures, whereas both the activation energy and pre-exponential factor decreased at the higher temperature region. Table 4 shows trend that the activation energy and the pre-exponential factor decrease with higher heating rate. Table 5 depicts that the activation energy and the pre-exponential factor increase with the addition of furnace gas flow rate.

Mixture	Temperature range (?C)	Fitting equation	r	E	A	n
L100	180–724	y = 6.6072 + 4.7904x	0.9928	39.8274	129.4	4.4
L75+RH25	180–371	y = 0.316 + 7.9352x y = 9.7047 + 2.5852x	0.9941	65.9733	1.158×10^{5}	4.4
	380–633		0.9795	21.4934	3.154	0.7
L50+RH50	180–361	y = – 5.4064 + 11.073x y = 2.0989 + 10.202x	0.9856	92.0609	4.935×10^{7}	4.4
	371–654		0.9885	17.4503	1.557	0.7
L25+RH75	180–370	y = – 9.9654 + 13.434x y = 10.341 + 1.8513x	0.9915	111.6903	5.717×10^{9}	4.4
	379–514		0.9604	15.3917	1.1953	0.6
RH100	180–397	y = – 10.422 + 13.813x y = 11.597 + 1.096x	0.9962	114.8413	0.928×10^{10}	4.4
	406–574		0.9689	9.1121	0.2015	0.7

r = correlation coefficient, E = activation energy (kJ/mol), A = pre-exponential factor (1/min), n = reaction order

Table 3: Fitting equations and kinetic parameters of Thai lignite, rice husk and their mixtures for different proportion.

Heating rate (?C/min)	Temperature range (?C)	Fitting equation	r	E	A	n
10	178–326	y = – 2.9372 + 9.5379x	0.995	79.2981	1.799×10^{6}	5
	336–616	y = 6.6074 + 4.1587x	0.9827	34.5754	56.15	1.1
20	180–371	y = – 1.2122 + 8.7939x y = 9.1268 + 2.9638x	0.9972	73.1125	5.911×10^{5}	5
	380–672		0.9884	24.641	6.444	0.8
30	179–390	y = 1.3999 + 7.5107x y = 11.542 + 1.4975x	0.9956	66.27	1.492×10^{5}	4
	399–708		0.9959	12.4502	0.436	0.5
40	183–394	y = 1.0441 + 7.8129x y = 11.755 + 1.3627x	0.9852	64.9565	1.1×10^{5}	3
	413–778		0.9974	11.3295	0.428	0.6

r = correlation coefficient, E = activation energy (kJ/mol), A = pre-exponential factor (1/min), n = reaction order

Table 4: Fitting equations and kinetic parameters of Thai lignite, rice husk and their mixtures for different heating rates.

Flow rate (ml/min)	Temperature range (?C)	Fitting equation	r	E	A	n
10	180–390	y = 0.807 + 7.8249x	0.9954	65.0562	6.983×10^{4}	5
	400–778	y = 12.246 + 1.056x	0.9931	8.7796	0.1015	0.5
20	180–390	y = 0.0781 + 8.1101x y = 11.279 + 1.6154x	0.9939	67.4274	1.501×10^{5}	5
	405–654		0.9984	13.4304	0.4082	0.5
30	180–360	y = – 0.2278 + 8.1999x y = 9.7114 + 2.5797x	0.9963	68.1739	2.061×10^{5}	5
	370–663		0.9949	21.4476	3.126	0.7
40	180–360	y = – 1.4137 + 8.7627x y = 7.0819 + 3.986x	0.9923	72.8531	7.205×10^{5}	5
	363–724		0.9726	33.1396	66.98	1.1

r = correlation coefficient, E = activation energy (kJ/mol), A = pre-exponential factor (1/min), n = reaction order

Table 5: Fitting equations and kinetic parameters of Thai lignite, rice husk and their mixtures for different furnace gas flow rates.

X. CONCLUSIONS

Thermogravimetric characteristics and specific temperatures of Thailignite, rice husk, and their mixtures have been investigated using a thermogravimetric analysis (TGA). The experimental results revealed excellent combustion properties of both selected fuels. However, rice husk exhibited higher thermal and combustion reactivity, compared to Thai lignite, andtherefore can be used as a secondary/reburn fuel in fuel-staged co-firing systems, leading to lower environmental impacts. The kinetic parameters obtained can be used for modelling the time-related decomposition of the fuels studied.

REFERENCES

[1] ElectricityGeneratingAuthorityofThailand."MaeMohpower plant". May 2018. Available athttp://www.egat.co.th/index.php?option=com_content&vie w=article&id=2494&Itemid=117.

[2] M.Sami,K. Annamalai,andM. Wooldridge,"Co-firingof coal and biomass fuel blends",Prog. Energy and Combust. Sci.,vol. 27, pp.171–214, 2001.

[3] P.NinduangdeeandV.I.Kuprianov,"Fluidized bed co- combustion of rice husk pellets and moisturized rice husk:The effects of co-combustion methods on gaseous emissions",Biomass Bioenergy, vol. 112, pp. 73–84, 2018.

[4] H.Haykiri-Acma,S.Yaman,andS.Kucukbayak, "Comparison of the thermal reactivities of isolated lignin and holocellulose during pyrolysis",Fuel Process. Technol.,vol. 91, no. 7, pp. 759–64, 2010.

[5] A. Gani and I.Naruse, "Effects of cellulose and lignin content on pyrolysis and combustion characteristics of several types of biomass", Renewable Energy, vol. 32, pp. 649–661, 2007.

[6] P. Ninduangdee,V.I. Kuprianov, E.Y. Cha, R. Kaewrath, P. Youngyuen,andW.Atthawethworawuth,"Thermo-gravimetric studies on oil palm empty fruit bunch and palm kernel shell: TG/DTG analysis and modeling",Energy Procedia, vol. 79, pp. 453–458, 2105.

[7] S.S.Idris, N.A. Rahman, and K."Combustion characteristics of Malaysian oil palm biomass, sub-bituminous coal and their respective blends via thermogravimetric analysis (TGA)",Bioresour Technol., vol. 123, pp. 581–591, 2012.

[8] H.Haykiri-Acma,S.Yaman,andS.Kucukbayrak,"Co- combustion of low rank coal/waste biomass blends using dry air or oxygen",Appl. Therm. Eng., vol. 50, pp. 251–259, 2013.

[9] V.Seebauer, J.Petek, and G. Staudinger. "Effects of particle size, heating rate and pressure on measurement of pyrolysis kineticsbythermogravimetricanalysis",Fuel,vol. 76, pp. 1277– 1282, 1997.

[10] P.Ninduangdee,V.I. Kuprianov, E.Y. Cha, R. Kaewrath, P. Youngyuen,andW.Atthawethworawuth,"Thermogravimetric studies on oil palm empty fruit bunch and palm kernel shell: TG/DTG analysis and modeling",Energy Procedia, vol. 79, pp. 453–458, 2105.

[11] A.W. Coats and J.P. Redfern, "Kinetic parameters fromthermogravimetric data",Nature,vol. 201, pp. 68–69, 1964.

Synergism of Thermal Conductivity Enhancement in Binary Polymer Matrix Binary Nano Particle Reinforced Composite

[1] R. A. Mizan, [2] M. A. Islam
[1]Graduate Student
[2]Professor, Department of Materials and Metallurgical Engineering, Bangladesh University of Engineering and Technology (BUET), Dhaka-1000, Bangladesh
E-mail: aminulislam@mme.buet.ac.bd

ABSTRACT

In recent years, high strength and low cost conductive polymer composites have attracted a considerable attention of worldwide researchers due to their wide range of applications. Usually, they are being made by adding high volume fraction of conductive reinforcing fine particles in polymers, which is expensive and also causes some problems as it reduces the moldability and draw ability of the composites. Binary polymer matrix with binary conductive particle reinforced composite could be a solution to overcome the challenges. This study is designed to develop a conductive binary matrix polymer composites composed of polymers of high strength (polypropylene, PP) and soft but conductivity friendly (ethylene-co-vinyl acetate, EVA) with relatively lower amount of conductive binary nano filler materials (carbon black and alumina powder). For doing this, samples were prepared by mixing all ingredients (PP 60wt%, EVA 40wt%) and their thermal conductivity values were measured. After detailed experimental study, it has been revealed that the thermal conductivity of the developed binary nano particle reinforced composite is nearly 12 times higher than that of the pure PP and 10 times higher that of pure EVA, whereas the conductivity is significantly lower if the reinforcing particles (carbon and alumina) are used separately.

Keywords - Polypropylene, Ethylene-Co-Vinyl Acetate, Binary Matrix, Binary Filler, Thermal Conductivity

I. INTRODUCTION

Among different types of polymers used, polypropylene is light, low cost, easy of processing and excellent chemical stability with high mechanical strength [1,2]. This polymer is not only used in plastic industries, but it is also used in bulk volume as fibres in textile industries. On the other hand, polymers like polyanylene, polyvinyl alcohol, polyethylene-co-vinyl acetate, etc have moderate to high thermal conductivity. Conducting polymeric materials also have a wide range of uses for making antistatic coatings, electromagnetic shielding materials, biomaterials, semiconductors and batteries [3,4,7,8]. As we know, PP has good mechanical properties, however, its conductivity is relatively poor. On the other hand, compared to PP, EVA has better thermal and electrical conductivities, but it is relatively soft. In this situation, binary matrix (PP and EVA) polymer could be a good choice for a more balanced mechanical and thermal property combination [9-11]. EVA added PP binary polymer has also drawn considerable attention to be used in smart fabric, which can give comfortness as well as high durability because of its relatively high strength [3-7]. Different particles are increasingly being used as

additives in polymers to simultaneously enhance a variety of properties without sacrificing other useful qualities of the base polymers. Carbon black, activated carbon and alumina, for example, have very high thermal and electrical conductivities. As a consequence, these fillers can be used to convert thermally and electrically insulating polymers into conductive materials [12-14].

II. MATERIALS AND EXPERIMENTAL PROCEDURE

For making binary polymer matrix PP and EVA along with two different fillers as carbon black and alumina powders were collected from the local market.

In development of the composite, at first, the ingredients of the binary polymer matrix (PP 60wt% and EVA 40wt%) along with 6wt% (compared to the total weight of PP and EVA) the nano filler particles (carbon black and alumina of particle size less than 100nm, Fig.1) singly or in combination (as binary filler material) were melted and blended in a simple polymer melting and blending unit having rotational speed range from 0 to 60 rpm and temperature range up to 450°C. To begin, all compounds ingredients were mixed at 190°C in the blending unit using a 30 rpm speed for 10min.

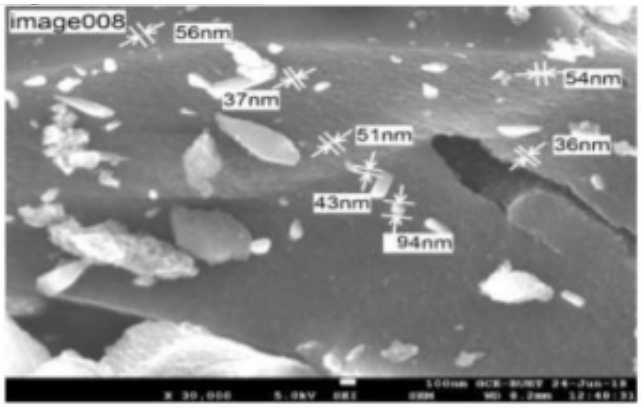

Figure 1: SEM photomicrograph showing the particle size of filler material.

The molten polymer from the blending machine was then transferred to an aluminum mold and the mold was then placed under a hot press. Thereafter, the samples were molded to plate shape by hydraulic compression press at a pressure of approximately 30kN for 5min at 190°C. After cooling, the cast sample was taken out from the mould (the overall operation in hot press is shown in Fig.2). The prepared samples were characterized by FTIR analysis, FEGSEM and thermal conductivity tests.

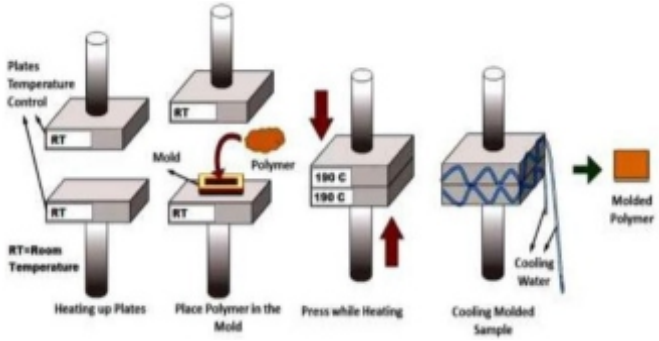

Figure 2: Schematic of sample preparation of compression molding in hot press.

III. RESULTS AND DISCUSSION

3.1. FTIR Spectroscopy

Figure 3 represents the FTIR spectra for the blended PP/EVA and filler materials, where all characteristics peaks have been found. The peaks found like 2914cm-1, 2847cm-1, 1730cm-1, 1464cm-1, 1375cm-1, 1300cm-1 and 720cm-1, respectively, represent methylene asymmetric C–H stretching, methylene symmetric C–H stretching, aliphatic C=O ester group of EVA, methylene scissoring, methyl symmetrical C–H bending, methylene wagging and methylene rocking respectively. From the spectra resented in Fig.3 no new peak other that the characteristic peaks related to EVA and PP has been observed. This finding is a proof that after melting and blending of the binary polymer matrix of PP and EVA did not form any new type of polymer, rather than they just remain as co-continuous phases. Similar observation has also been mentioned by some other investigators [10,15].

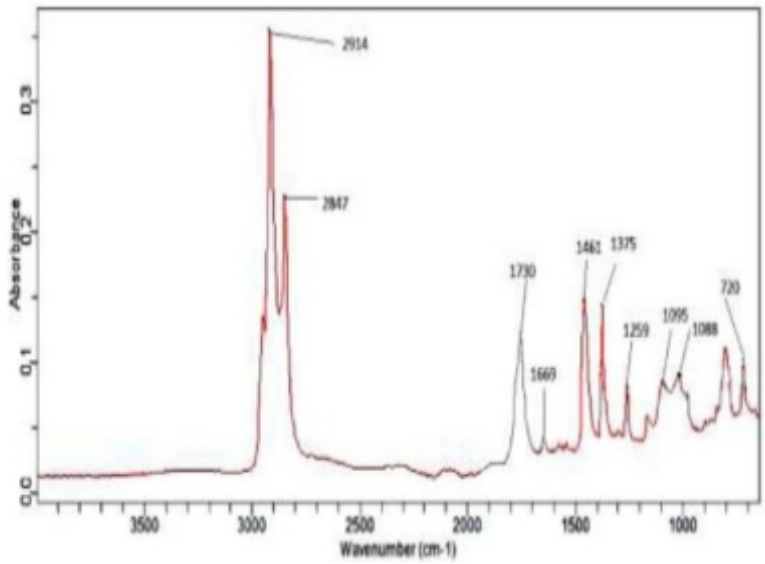

Figure 3: FTIR spectra binary polymer reinforced with binary particle.

Microstructural Observation in FEGSEM

The FEGSEM observation is presented in Fig.4. From this photomicrograph taken on tensile fracture surfaces, it is very clear that the two phases of PP and EVA are not in mixed condition, they just overlapped with each other creating a mating interface. PP is relatively brittle, which has been identified by its nature of brittle type of fracture, whereas EVA phase has been identified from its ductile nature of fracture mode. This observation figures out that these two polymers remain immiscible in the case of their binary matrix.

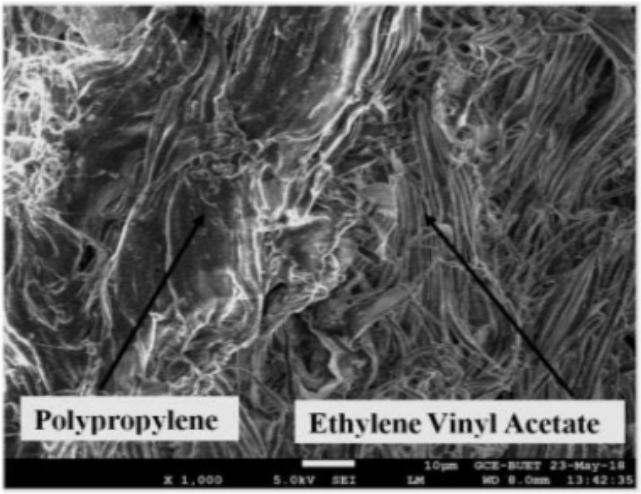

Figure 4: Immiscible phases PP and EVA binary matrix polymer.

Thermal Conductivity

Throughout the study binary matrix system of polypropylene (PP, 60 wt%) and ethylene vinyl acetate (EVA, 40 wt%) were used. The samples were designed in such way that single to binary particle effects on thermal conductibility of the developed composites could be possible to observe. Figure 5 indicates that the thermal conductivity of the binary polymer composites increase with the increase in the activated carbon filler content and that after adding about 8% of carbon particles the thermal conductivity increase from the value of base binary polymer matrix 0.16 to 0.9w/m.k. This increase might have been attributed due to continuous thermal pathways created in the composites.

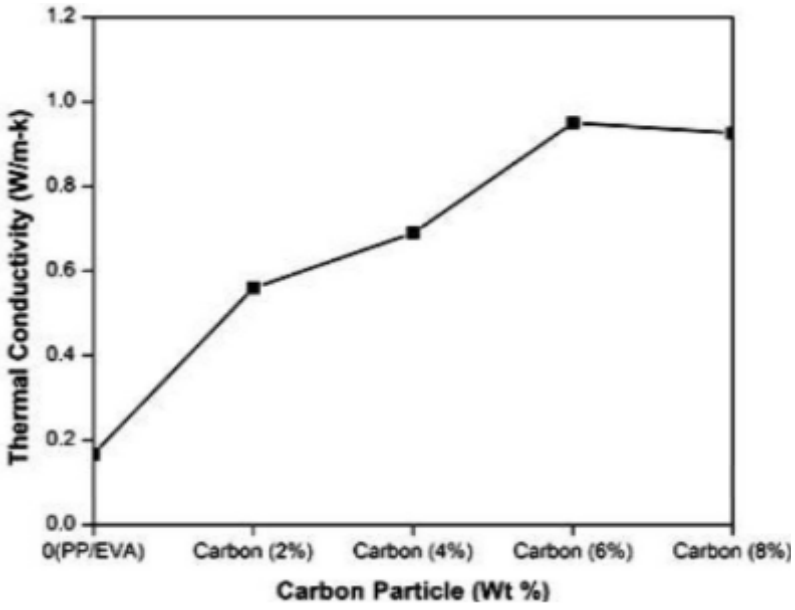

Figure 5: Variation of thermal conductivity with carbon particle content in PP and EVA binary matrix.

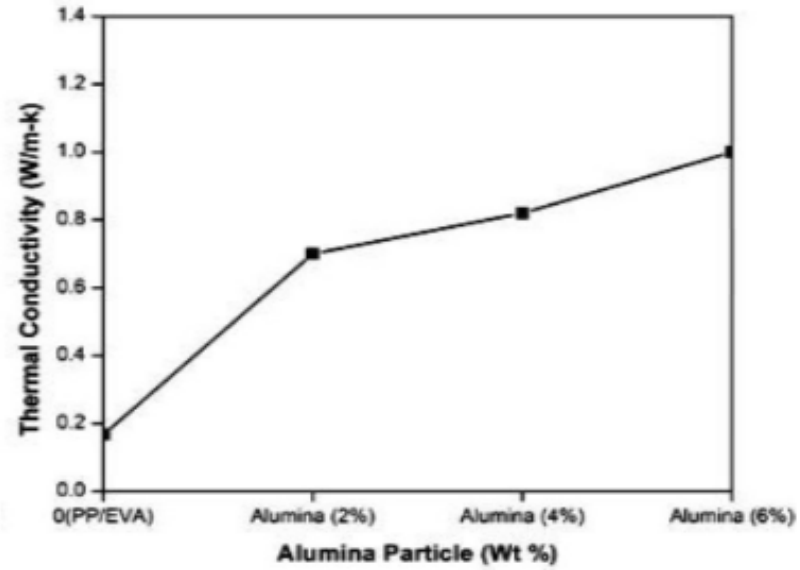

Figure 6: Variation of thermal conductivity with alumina particle content in PP and EVA binary matrix

Similar to activated carbon, alumina particle individually also has low effect on thermal conductivity of the composite (Fig.6), where the thermal conductivity increased from 0.16 to 1.0w/m.k after addition of 6% of filler particle. Slightly better conductivity increase has been possibly due to its higher thermal conductivity compared to that of the activated carbon particle. From Figs.5 and 6, it is clear that the effect of 6% alumina particle is very close to that of 8% carbon particle.

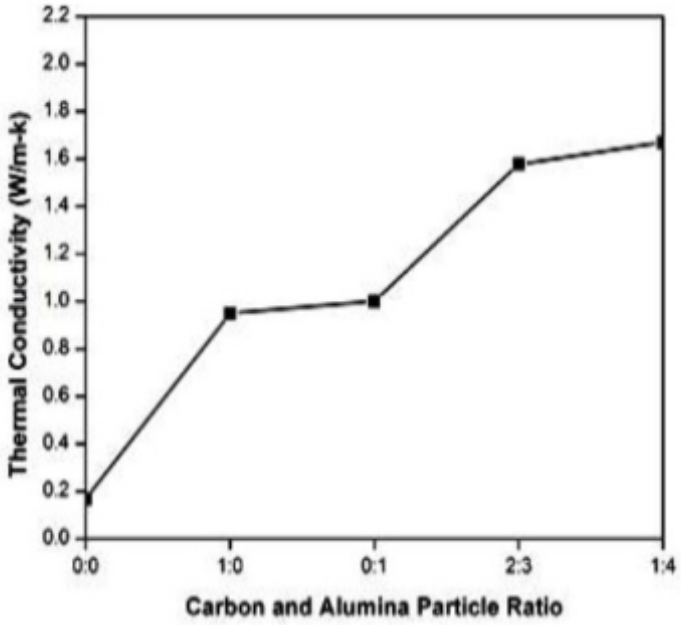

Figure 6: Variation of thermal conductivity of alumina and carbon binary particle content in PP and EVA binary matrix.

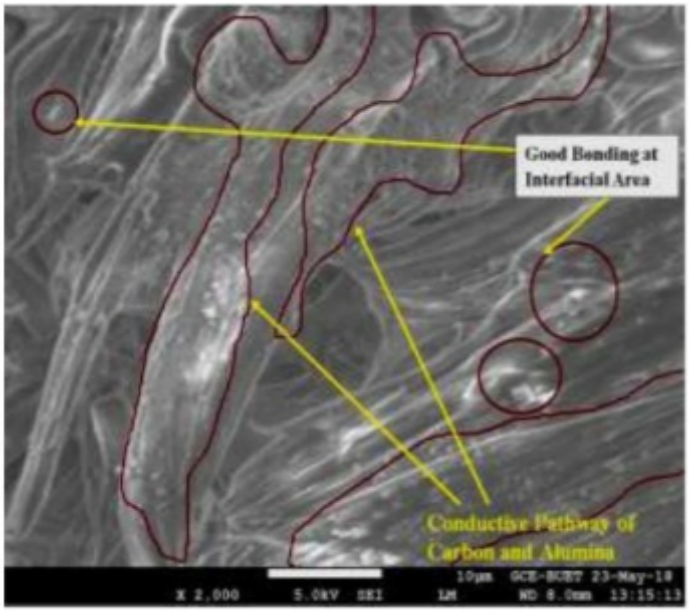

Figure 7: Easy conductive pathways in EVA phase in the binary PP and EVA polymer matrix.

For binary polymer matrix with binary particle reinforcement composite system the senerio is somewhat different, Fig.7. In the latter case, initially the thermal conductivity increases slightly similar to the single particle reinforced composite due to isolated alumina particle segregation in activated carbon particle. However, the trend has been changed when the alumina content is gradually increased as higher alumina created more continuous networks in immiscible interfacial zone of EVA. This is because EVA is polar materials, whereas PP is non-polar, where alumina particles tend to remain preferentially distributed in EVA phase, Fig.7. Consequently, more and favourable easy thermal pathways have been created in the composite. The carbon particles also create more contact between the alumina networks, which also accelerated the thermal conductivity of the composite. In this case the thermal conductivity has been increased to 1.7w/m.k from the base value of 0.16w/m.k, which is about 12 time higher than that of pure PP and 10 higher than that of pure EVA. Some other researchers have also mentioned similar observation [15,16]. Here it is to be noted that the thermal conductivity of pure PP and EVA are, respectively, 0.14w/m.k and 0.16w/m.k [17].

IV. CONCLUSION

In the present research, binary matrix by single particle and binary matrix by binary particle composites were fabricated with hot press technique following pre melting and blending of fixed 6wt% of filler. After development of the composite; it was characterized by FTIR spectroscopy, FEGSEM and thermal conductivity tests. After the detail investigation the followings outcome can be concluded from this work:

a. The polymer composite containing single filler either organic particle (activated carbon) or inorganic particle (alumina) have lower effect on thermal conductivity of polymer composite than binary particle.

b. It is revealed from experimental result that in the binary matrix immiscible co-continuous phase of binary matrix of PP/EVA has been formed that helped to particle distribution in immiscible interfacial zones of the binary matrix. This creates thermal conductive pathways of filler that caused significant enhancement in the thermal conductivity. The ultimate thermal conductivity of this study is nearly twelve times of the pure PP and ten times of pure EVA having 6wt% of filler in the binary matrix system.

ACKNOWLEDGEMENT

The authors would like to express their gratitude to CASR of BUET to provide necessary fund and research facilities to conduct this research work. They also indebted to MME Departmant for ensuring the use of all laboratory facilities.

REFERENCE

[1] Okada and A. Usuki, "Twenty years of polymer clay nanocomposites," Macromolecular Materials and Eng-ineering, vol.291, no.12, pp.1449-1476, 2006.

[2] Utracki, S. Maryam and E. Boccaleri, "Synthetic, Layered Nanoparticles for Polymeric Nanocomposites", Polymers for Advanced Technologies, vol.18, no.1, p.1-37, 2007.

[3] Ramadan, R.A. Mohamed and K.H Mohamed ,"An Idea to Enhance the Thermal Performance of HDPE Pipes Used for Ground-source Applications", Thermal Engg., vol.109, pp.15-21, 2016.

[4] Q. Li, J. Lu, X. Zeng, R. Sun, J. Wu, J.B. Xu, and C.P. Wong, "Enhanced Thermal Conductivity for Ag-deposited Alumina Sphere/Epoxy Resin Composites Through Manipulating Interfacial Thermal Resistance", Composites Part A: Applied Sci. and Manufacturing, vol.107, pp.561-569, 2018.

[5] Agrawal and A. Satapathy, "Effects of Aluminium Nitride Inclusions on Thermal and Electrical Properties of Epoxy and Polypropylene: An Experimental Investigation", Composites Part A: Applied Sc. and Manufacturing, vol.63, pp.51-58, 2014.

[6] L. Liu, P. Li, L. Ding, W. Tong, F. Li and Y. Zhang, ''Utilization of Industrial Ultra fine Carbon Ash as Filler of High k Composites with High Density Polyethylene as Matrix", Environmental Progress & Sustainable Energy, vol.36, no.6, pp.1719-1724, 2017.

[7] Liming, "Intelligent Macromolecules for Smart Devices: from Materials Synthesis to Device Applications", Springer Sci. & Business Media, 2004.

[8] P. M. Ajayan and H. S. Nalwa, "Handbook of Nanostructured Materials and Nanotechnology", Academic Press, New York, 2000.

[9] Paul and C. Bucknall, "Introduction in Polymer Blends Formulation", vol.1, 2000.

[10] Laurent and L. Leibler, "A Model for Toughening of Semicrystalline Polymers", Macromolecules, vo.40, no.15, pp.5606-5611,2007.

[11] S. Surajit, "Model Aircraft", Mega Hobby.com, 27 July 2013, www.megahobby.com/categories/model-aircraft.html.

[12] Orna and S. Uttandaraman, "Big Returns from Small Fibers: A Review of Polymer/Carbon Nanotube Composites, Polymer Composites, vo.25, no.6, pp.630-645, 2004.

[13] N. James and P. Krzysztof, "Polymer Nanocomposites for Aerospace Applications", Advanced Engg. Materials, vol.5, no.11, pp.769-778, 2003.

[14] R. S. Prasher, J.Y Chang, I. Sauciu, D. Chau, G. Chrysler and C. Hu, "Nano and Micro Technology-Based Next-Generation Package-Level Cooling Solutions", J. Intel Tech., vo.9, no.4, pp.205-211, 2005.

[15] M. Sarikanat, K. Sever, Y. Seki, and I. Özdemir. "Preparation and Mechanical Properties of Graphite Filled HDPE Nanocomposites", Arch. Mater. Sci. Eng, vol.50, no.2, pp.120-124, 2011.

[16] O. Abdollah and A.A. Rostami, "The Effects of Alumina Nanoparticle on the Properties of an Epoxy Resin System", Materials Chemistry and Physics, vo.114, no.1, pp.145-150, 2009.

[17] Properties of Polymers, Fourth Edition 2009, Elsevier Publisher.

Thermal Comfort Evaluation of A Building Under A Naturally Ventilated Environment in A Hot Climate

[1] Shian Gao, [2] Sherzad Hawendi, [3] Ahmed Qasim Ahmed
[1]Department of Engineering, University of Leicester, LE1 7RH, United Kingdom
[2]University of Sulaimani, Sulaimani, Kurdistan Region, Iraq
[3]Engineering Technical College, Middle Technical University, Baghdad, Iraq
E-mail: [1]sg32@le.ac.uk, [2]sherzadma@hotmail.com, [3]en_ahmed82@yahoo.com

ABSTRACT

In this study, the natural ventilation potential of residential buildings to provide suitable thermal comfort for occupants was numerically investigated based on an isolated family house in a hot climate. Computational Fluid Dynamics (CFD) technique is used to investigate the effects of the outdoor conditions, on human thermal comfort. The results of this study show that it is possible to implement natural cross-ventilation in domestic buildings and provide occupants' thermal comfort without the use of mechanical cooling. The results of the study suggest that acceptable thermal conditions can be maintained with the external wind speeds ranging from 2 to 5 m/s at the temperature of 25°C. In addition, the study has predicted the range of wind temperatures that would allow for all rooms in the building to be of acceptable thermal comfort, in the range of 22-28°C for the seated plane, and 20-28°C for the standing plane, when the external wind speed is 3 m/s.

Keywords - Natural Ventilation, Thermal Comfort, Computational Fluid Dynamics (CFD).

I. INTRODUCTION

Natural ventilation has become an increasingly attractive proposition for the reduction of energy usage and cost whilst still providing an acceptable quality of indoor environment and preserving a comfortable, healthy, and productive indoor climate rather than the more prevalent approach to the use of heating, ventilation and air-conditioning (HVAC) systems that in turn fail to reduce carbon emissions [1].

A successful design for a naturally ventilated building needs to be balanced in terms of three main factors: indoor air quality, thermal comfort and energy consumption [2]. Thermal comfort is the condition which expresses the level of satisfaction with the thermal environment and is usually assessed by subjective evaluation; there are many factors that affect thermal comfort such as heat conduction, convection, radiation, evaporative and heat loss [3]. Factors that have a large influence on thermal comfort are usually divided into two groups; (i) personal factors related to the occupants' levels, and (ii) environmental factors, e.g., conditions related to the thermal environment such as airspeed, humidity, outdoor temperature, metabolic rate and clothing level [4]. In the building sector alone, the interest regarding energy-consciousness and sustainable eco- building development has increasingly grown to gain a better indoor environment and reduced energy consumption [5].

Therefore, there have been numerous indoor thermal environmental studies conducted for various types of buildings, including public buildings, transportation, whole building environments, offices and specific enclosed spaces; one common feature of these studies is the evaluation of thermal comfort [6].

Indoor thermal comfort is determined by various factors in the current study, with Predicted Mean Vote (PMV) and Predicted Percentage of Dissatisfied (PPD) being two such factors considered. Occupants can control their indoor thermal environment by clothing, operable windows, fans or heaters, and sun shades.

ASHRAE Standard 55 uses the PMV and PPD indices to set the requirements for the indoor thermal comfort, and it predicts the mean value of the votes for a large group of subjects for a particular combination of air and radiant temperature, clothing insulation, metabolic rate, air speed, and relative humidity. Standard thermal comfort surveys ask subjects about their impression as to their thermal sensation on a seven-point scale of cold (-3) to hot (+3), where zero is the ideal value with recommended limits between (-0.5) and (0.5) [3], in which 90% of people claimed to be comfortable, respectively [6].

The mathematical expression of Fingers' PMV model is as given by Eq. 1 below [7]:

$$=[0.303-0.036+0.028]\{(-)-3.96-8[(+273)4-(+273)4]-h(-)-3.05[5.73-0.007(-)-]-0.42[(-)-58.15]-0.0173(5.87-)-0.0014(34-)\} \quad =100-95[-(0.03353\,4+0.2179\,2)]$$

where tcl (°C) is the surface temperature of clothing, tr (°C) is the mean radiant temperature, fcl is the clothing area factor, pa (kPa) is the partial water vapor pressure and hc (W/m^2C) is the convective heat transfer coefficient between the occupant and the environment. The Finger's Equation and all equations that used for calculating tcl, fcl, pa and hc were written in the UDF file (User-Define-Function) and linked with ANSYS FLUENT.

Given the climate of Kirkuk city in the north of Iraq, the mechanical cooling of buildings is required during the summer while during the spring and autumn seasons natural ventilation can be introduced by using various passive methods including window opening, stack effects and night ventilation. These methods should be tested in order to find an active way to maximize the comfort of occupants. The main objective of this study is to quantify the impact of outdoor weather conditions (wind speed and temp-erature) on the human thermal comfort indices (PMV and PPD) of an isolated family house in Kirkuk under a natural ventilation environment in a hot climate. The impact of outdoor weather

conditions on the thermal comfort indices is analysed through a series of CFD simulations. The low Reynolds number (LRNM) with Steady Reynolds Averaged Navier–Stokes (RANS) R N G k - modelling approaches are employed in these simulations. The CFD model was validated against available data from wind tunnel experiments [8] in previous studies [9, 10]. The findings from the study are expected to improve our understanding and knowledge as to the impact of these parameters on the human thermal comfort indices in residential buildings.

II. DBUILDING GEOMETRY

The motivation behind this study is to evaluate the potential for natural ventilation to determine a suitable level of thermal comfort for occupants in an isolated family house in Iraq which consist of five rooms: kitchen (A), sitting room (B), living room (C), and two bedrooms (D & E), as shown in Fig.1 and the dimensions are shown in Table 1. This layout is simple and represents an average house for an average family in Iraq [9]. The height of the building was H, with base dimensions of (3.33×2.66) H, with two square openings (0.2 H) in the front wall and two openings at the rear of the building, and the wall porosity (opening area divided by wall area) was 3%. The building has an external boundary wall and the height of the wall was 0.33H. The thickness of the walls was 0.067H, and the length of the building was less than the maximum length suggested by Chu et al. [11] to obtain effective wind-driven cross ventilation. The wind speed was based on the reference at the height of the building (Uref) with an angle of incidence of 0o.

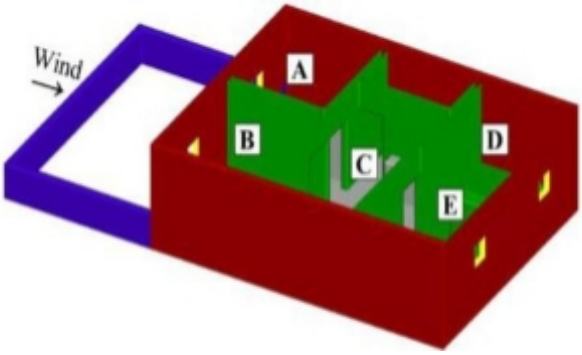

Fig. 1 The geometry of the building model.

Room	Room type	Dimension size (L×W) in meters
A	Kitchen	(3.2×3.4)
B	Sitting room	(3.2×4.0)
C	Living room	(3.0×5.9)
D	Bedroom I	(3.0×3.4)
E	Bedroom II	(3.0×4.0)

Table 1: Dimensions of the rooms.

III. COMPUTATIONAL MODEL SETTING AND PARAMETERS

The computational domain was constructed based on the guidelines in wind engineering, and had dimensions (23.33×5×12.6) H. The building was set inside the duct, the blockage ratio was 4.2%, and the distance between the outflow boundary and the building was 15H, which is enough to allow the flow to redevelop in the wake region. The numerical grid used consisted of around 6×106 hexahedral computational cells, with a fine mesh structured near the walls of minimum grid spacing 0.005H, whereas a coarse mesh was used away from the walls. A grid independence study for the basic case was conducted to ensure that the results were independent of the mesh resolution; a logarithmic inlet velocity profile was employed at the inlet of the duct, with the equations of turbulent kinetic energy and specific dissipation rate equations reported in the previous study by the current authors [9, 10, 12]. The surfaces of the building and the ground of the domain were modelled as no-slip boundaries, while symmetric boundary conditions were applied to the two sides and top of the domain, and outflow boundary conditions were specified at the end of the domain.

The walls in the house geometry were assumed adiabatic. A uniform temperature was specified as the outdoor thermal condition and was applied to the inlet boundary of the duct. The heat generation was uniformly applied to the floor of all the rooms as a boundary condition, and was assumed as 100 W/m2 for a family house with several occupants using several electrical appliances at any given time [6]. For incompressible flow, the pressure-based solver was used in the current study. The SIMPLEC scheme was imposed as the pressure–velocity coupling method.

IV. RESULTS AND DISCUSSION

The numerical results are presented and compared in terms of velocity and temperature, followed by the human thermal comfort indices (PMV and PPD). The investigation into outside weather conditions would give the designer valuable information in obtaining more energy-efficient designs in naturally ventilated buildings. The area of the openings in all cases was kept constant, as was the wind incidence angle of 0o.

The thermal comfort indices predicted for metabolic rates, M, were 58 W/m2 (seated), and 70 W/m2 (standing). The thermal resistance due to typical clothing insulation in spring and autumn conditions was set to be equal to 0.6 clo, whilst the relative humidity was fixed at 30% with zero external work (W). The room average PMV, PPD, velocity and temperature of a horizontal plane at a height of 0.6 m from the ground of the building were calculated for the seated case as recommended by ASHRAE 55 [3] and 1.1 m for the standing case according to the International Organization for Standardization (ISO 7730:2005) [13].

Impact of outdoor wind speed

The impact of outdoor wind speed on the indoor thermal comfort was studied by using reference wind speeds (Uref) of 1 to 6 m/s at the building height H, whilst the temperature was fixed at 25°C. The numerical results are presented and compared in terms of average velocity and temperature, followed by PMV and PPD for the seated level and sanding levels. Fig. 2 and Fig. 3 show the PMV, PPD, average velocities, temperatures, in the seated plane 0.6 m above the floor. Under the reference velocity of 3 m/s, the seated plane was found to have an average velocity of 0.16 m/s and acceptable thermal comfort with a PPD of around 11%, whereas at a Uref of 1 m/s the PPD increased to higher than 33% and the average velocity decreased to lower than 0.06 m/s, resulting in warm conditions inside the building. When Uref was 6 m/s, the average velocity of the plane increased to 0.35 m/s, decreasing the average temperature by around 1°C and resulting in a high PPD of 22%, though the plane still had acceptable thermal comfort (-1 < PMV > +1). In addition, the wind-driven ventilation delivered a low air velocity for the rear rooms (D and E) with an average of approximately 0.1 m/s at the Uref of 3 m/s and high air velocity for the front rooms (A and B) of 0.25 m/s at the same reference velocity, therefore significant differences appeared between these rooms in terms of thermal comfort. For instance, the differences between the front rooms A and B and the rear rooms D and E of PPD were 4% when Uref was 3 m/s, while in the case where Uref was 6 m/s this difference increased to 34%. It can also be seen that the difference in the thermal index (PPD) for the front rooms was higher than that for the rear rooms by 45% at a reference velocity of 1 m/s. This is because, at high velocity, the differences in temperature between the front and rear rooms were small and the differences in velocity were high, thus the velocity was thought to become more influential than the temperature in creating these differences in values of thermal comfort indices between these rooms. At low velocity, the differences in temperatures were high between the front and rear rooms and differences in velocities were small; therefore, the temperature was thought to become more influential on the thermal comfort indices, as shown in Fig. 1. The small differences in of PPD at Uref of 3 m/s between the front and rear rooms lead us to conclude that the building will be in a good comfortable thermal condition at reference velocities of around 3 m/s.

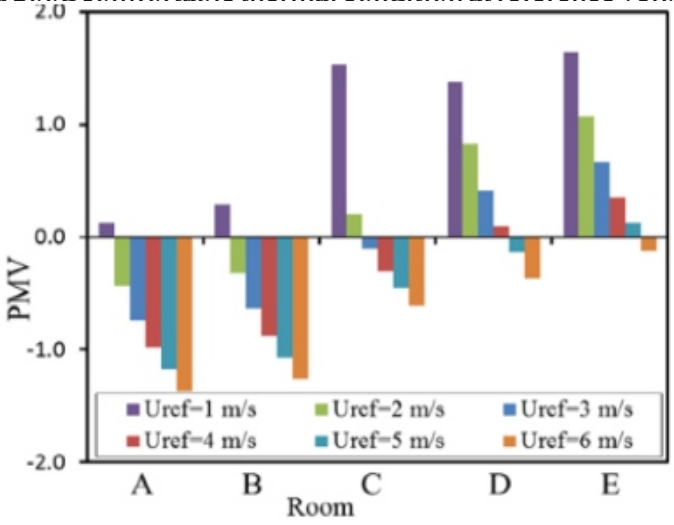

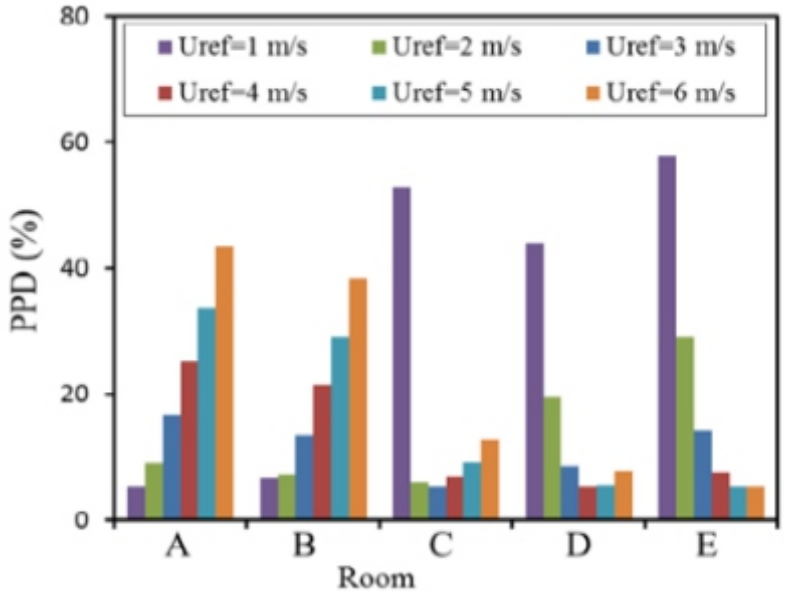

Fig. 2 The room average PMV and PPD in the seated plane.

The thermal comfort indices, average velocity and temperature for standing activities at a height of 1.1 m were also analysed, the results of which are presented in Fig.4 and Fig.5. The results showed the same trend as the seated level, despite the level of this plane being located nearer to the level of the opening positions than the seated plane. The average velocities for the standing plane were almost the same as the average velocity for the seated plane because both levels are distant to some extent from the opening positions' level, whilst the change in thermal comfort indices occurred because of the higher assumed metabolic rate in this plane than the seated plane. However, when the reference velocity was set to 3 m/s, the PPD for the seated and the standing planes were small, while significant differences in PMV were noted at a low Uref of 1 m/s and high Uref of 6 m/s. This means that at a reference velocity between 2-5 m/s the human thermal comfort zone (between the seated level and standing level) is in an acceptable thermal condition. Generally, it can be concluded that cross ventilation can provide an acceptable thermal comfortable environment for thistype of building as long as the wind speed ranged between 2-5 m/s, despite there being a few locations inside the house where PMVs were still higher than the acceptable range.

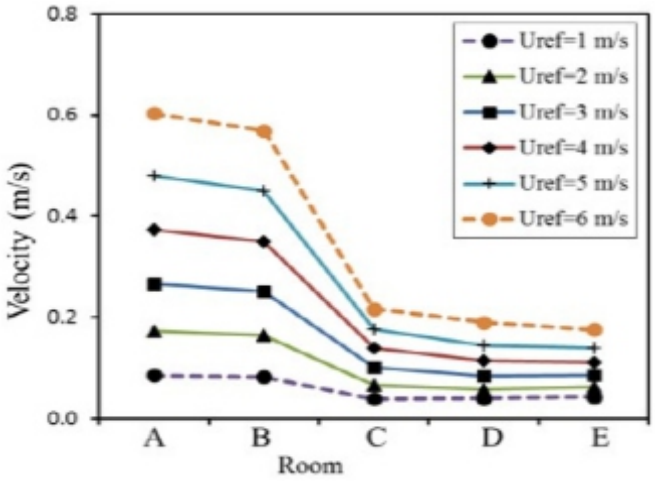

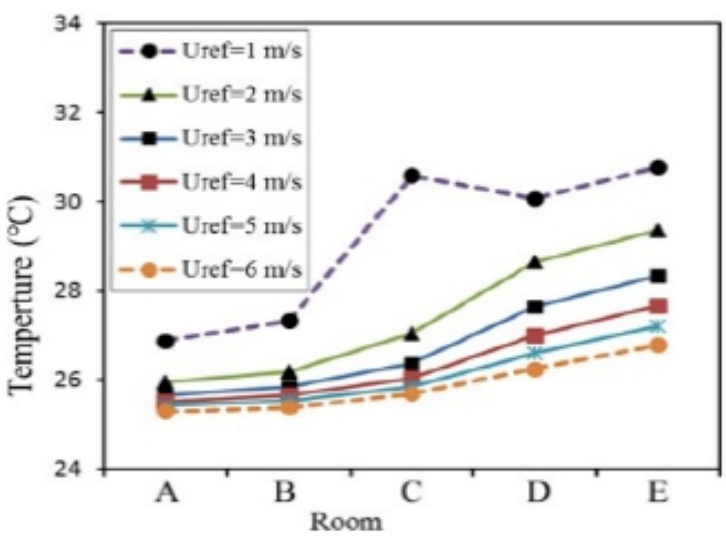

Fig. 3 The room average velocity and temperature in the seated plane.

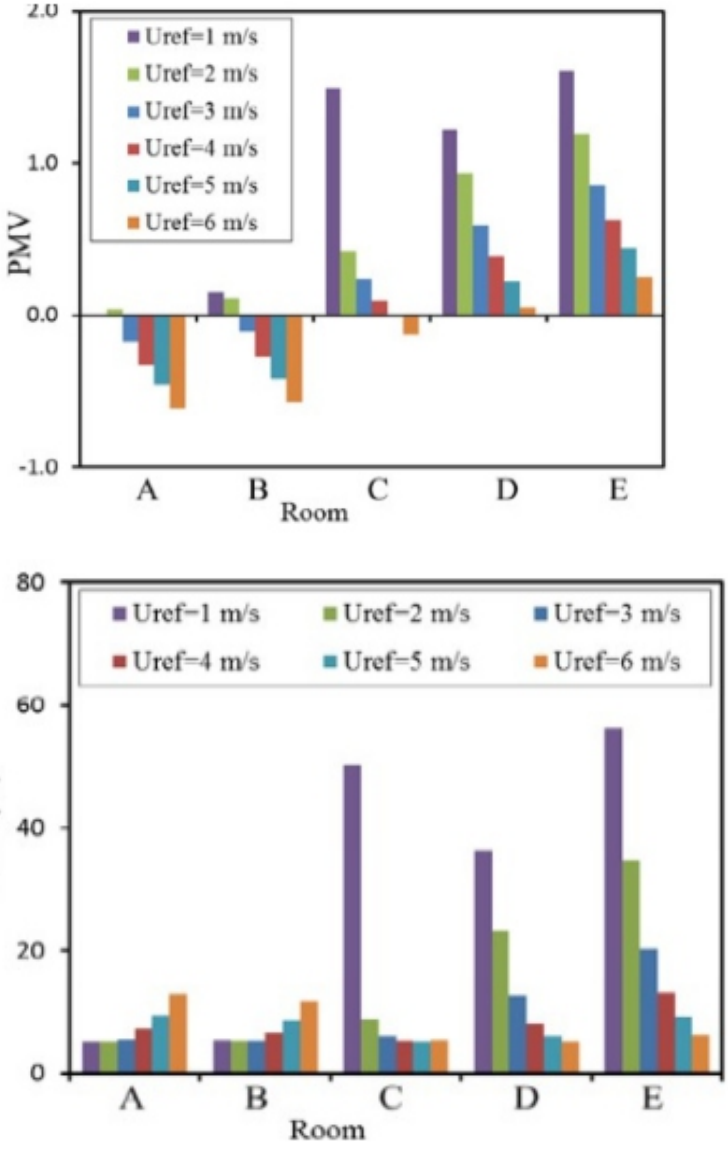

Fig. 4 The room average PMV and PPD in the standing plane.

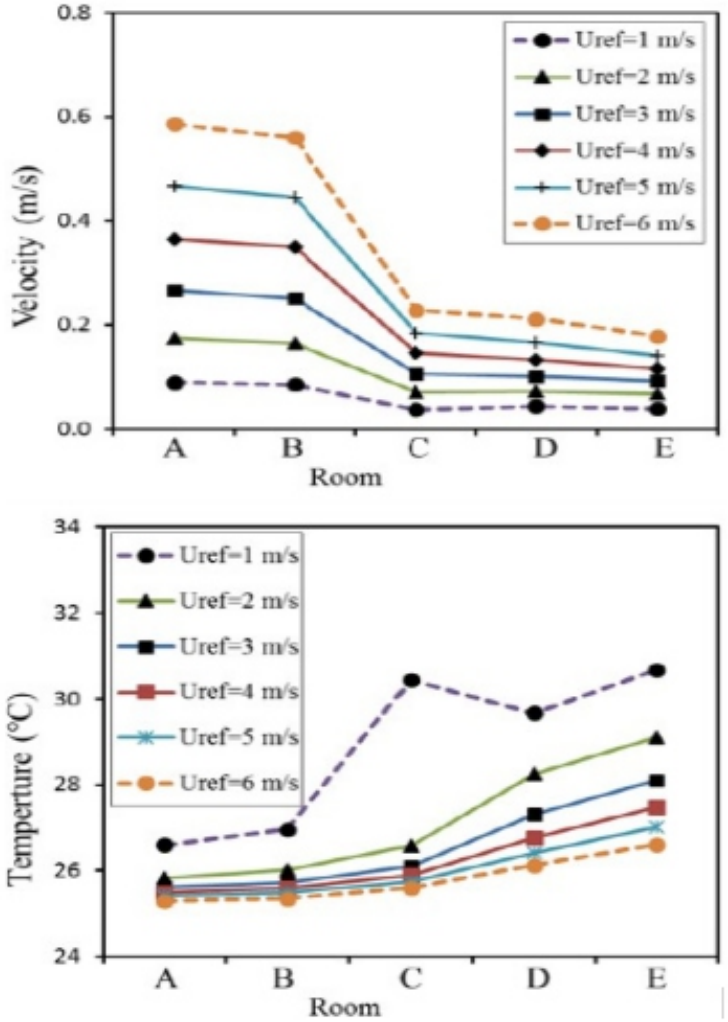

Fig. 5 The room average velocity and temperature in the standing plane.

Impact of outdoor wind temperature

The impact of ambient temperature on indoor thermal comfort is studied in this section. Case-III was chosen as a reference under a fixed wind speed of 3 m/s and with the ambient temperature changed from 20 to 29°C. Fig.6 shows the average PMV and PPD in each room of the building in both the seated and standing planes. The results showed that the operative wind temperature that provided the best thermal comfort in the seated plane was 25°C, where all rooms were in a comfortable condition and the PPD was around 11%. The PMV values remained close to comfortable conditions when the temperature increased to 27°C or decreased to 24°C and the PPD for the rooms in the seated plane raised to 20% which is reasonably good, though a high PMV was predicted in the rear rooms as discussed previously, while the thermal conditions changed to slightly warm/cool when the outside air temperature increased to 28°C or decreased to 23°C, respectively.

The results for the standing plane showed that a range of outside wind temperatures between 22-26°C can provide an acceptable PMV of +1 to -1 inside all rooms, i.e., between slightly cool and slightly

warm, while the rooms remain very comfortable when the wind temperature is at 24°C and close to neutral conditions for PMV when increased to 25°C or decreased to 23°C and the PPD for the rooms was less than 10%, implying that about 90% of the occupants would probably not find the thermal conditions uncomfortable. Overall, natural ventilation can be applied to this type of building across a rangeof wind temperatures between 22-28°C for the seated plane and 20-28°C for the standing plane. Thus, the conditions can be described as being between slightly cool and slightly warm.

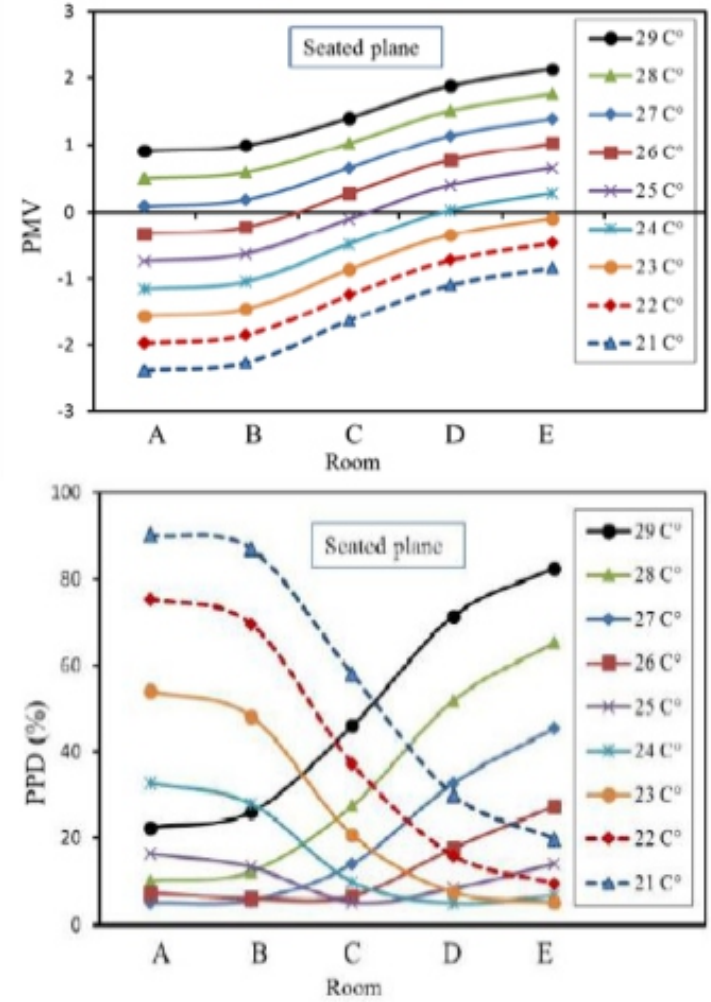

Fig. 6 The room average PMV and PPD in the seated plane.

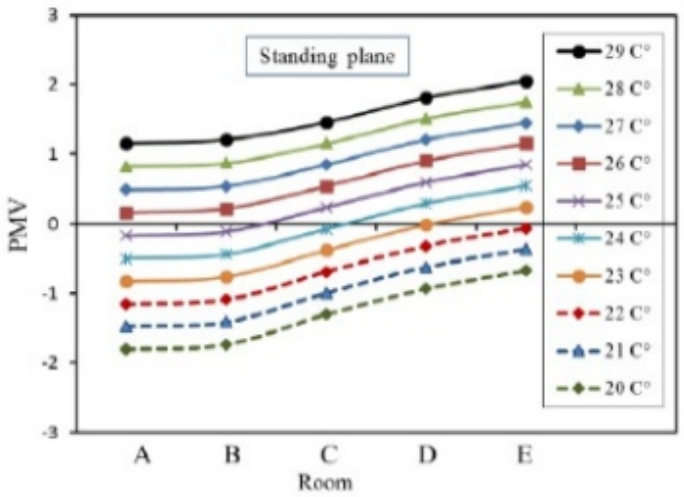

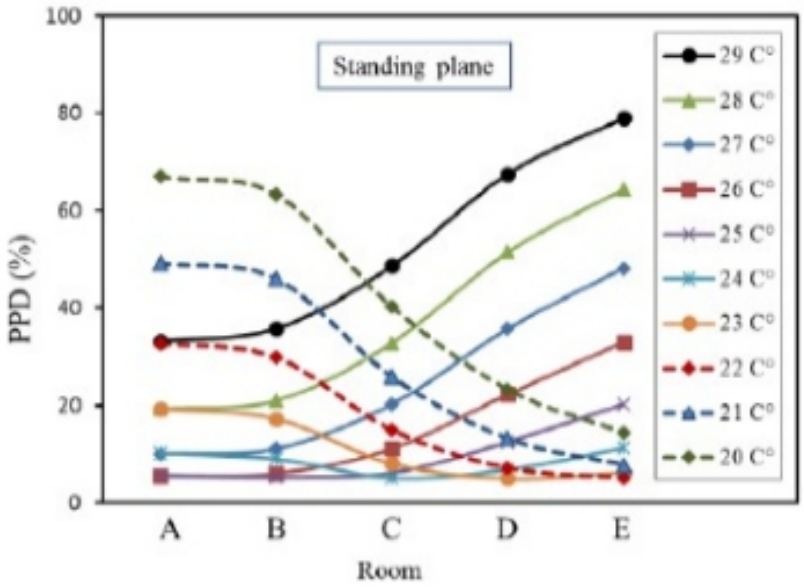

Fig. 7 The room average PMV and PPD in the standing plane.

V. CONCLUSIONS

The study has identified a gap in the knowledge regarding the control of natural cross-ventilation and the identification of the external conditions under which a natural ventilation system could maintain thermally comfortable internal environments for an average family house in a hot climate. The study uses CFD techniques to compare the flow and temperature fields for the cross-ventilation that use four openings and different opening arrangements. Compared to previous studies, there are new contributions to the studies on the thermal comfort in buildings under a natural cross-ventilation, as follows:

1. The study concludes that the cross ventilation can provide acceptable thermal comfort for this type of building when the wind speeds are between 2 and 5 m/s at the temperature of 25°C.
2. The study has demonstrated that the range of wind temperature conditions under which all the rooms in the house can be maintained within an acceptable thermal comfort range for the seated levels is between 22-28 °C and for the standing planes is between 20-28 °C with an external wind speed of 3 m/s.

The results of this study show that it is possible to implement natural cross-ventilation in a family house and provide occupants' thermal comfort without the use of mechanical cooling. As the current study considered only the two seasons, further research is needed to investigate the variation of natural ventilation potential across the whole of the year.

ACKNOWLEDGMENTS

The financial support for the project from the Ministry of Higher Education and Scientific Research of Iraq is gratefully appreciated.

REFERENCES

[1] G.C. da Graça, P. Linden, Ten questions about natural ventilation of non-domestic buildings, Building and Environment, 107 (2016) 263-273.

[2] Y. Xing, N. Hewitt, P. Griffiths, Zero carbon buildings refurbishment—A Hierarchical pathway, Renewable and sustainable energy reviews, 15(6) (2011) 3229-3236.

[3] A.S. ASHRAE, Standard 55-2013, Thermal Environmental Conditions for Human Occupancy, (2013).

[4] N. Al-Awainati, M.I. Fahkroo, F. Musharavati, S. Pokharel, H.A. Gabbar, Evaluation of thermal comfort and cooling performance of residential buildings in arid climates, Smart Energy Grid Engineering (SEGE), 2013 IEEE International Conference on, IEEE, 2013, pp. 1-6.

[5] K. Horikiri, Y. Yao, J. Yao, Numerical optimization of thermal comfort improvement for indoor environment with occupants and furniture, Energy and Buildings, 88 (2015) 303-315.

[6] S. Hawendi, Numerical investigation of thermal comfort in an isolated family house under natural cross-ventilation, PhD. Thesis, University of Leicester 2018.

[7] O.E. Abiodun, Examination of thermal comfort in a naturally ventilated hostel using PMV-PPD model and field survey, American Journal of Engineering Research, 3 (8)(8) (2014) 63.

[8] M. Ohba, K. Irie, T. Kurabuchi, Study on airflow characteristics inside and outside a cross-ventilation model, and ventilation flow rates using wind tunnel experiments, Journal of Wind Engineering and Industrial Aerodynamics, 89(14) (2001) 1513-1524.

[9] S. Hawendi, S. Gao, Investigation of Opening Positions on the Natural Ventilation in a Low-Rise Building by CFD Analysis, Proceedings of the 3rd International Conference on Fluid Flow, Heat and Mass Transfer (FFHMT'16, Paper No.151), Ottawa, Canada 2016.

[10] S. Hawendi, S. Gao, Impact of an external boundary wall on indoor flow field and natural cross-ventilation in an isolated family house using numerical simulations, Journal of Building Engineering, 10 (2017) 109-123.

[11] C.-R. Chu, B.-F. Chiang, Wind-driven cross ventilation in long buildings, Building and Environment, 80 (2014) 150- 158.

[12] S. Hawendi, S. Gao, Impact of windward inlet-opening positions on fluctuation characteristics of wind-driven natural

[13] cross ventilation in an isolated house using LES, International Journal of Ventilation, (2017) 1-27.

[14] P. ISO, 7730 Ergonomics of the thermal environment, Analytical determination and interpretation of thermal comfort using calculation of the PMV and PPD indices and local thermal comfort criteria, London: British Standards Institution, p.10. (2005).

Thermal Simulation of Multi Sparks Electric Discharge Deposition Process

[1] Deepak Kumar Prasad, [2] H Chelladurai
[1,2]Mechanical Engineering Department PDPM IIITDM Jabalpur
E-mail: [1]deepakkumar1540@gmail, [2]chella@iiitdmj.ac.in

ABSTRACT

This paper studies about the effect of input parameters on the thermophysical property of the copper electrode and deposition parameters for multi discharge electric discharge deposition (EDD) process. Copper is taken as tool electrode and stainless steel is taken as a workpiece. For deposition of copper, ZNC die sinker EDM with reverse polarity has been used. Finite element analysis software COMSOL Multiphysics has been used to understand the thermal and deposition model. Air is used as dielectric to avoid the bubble formation, which is not favorable for EDD. A plasma channel is established between tool and workpiece, which liberates high heat energy. This energy is involved in melting and vaporization of tool and workpiece material. The temperature distribution in the copper electrode is observed during the multi discharge. The main reason for the deposition of material is temperature. When the temperature of the electrode reached to melting point temperature, electrode gets melt and deposited over the substrate. In the deposition, the process temperature is the very first parameter and analyzed for different input parameters.

Keywords - EDD, Electrode gap, Air, Dielectric, COMSOL Multiphysics.

I. INTRODUCTION

Electric discharge deposition is one of the recently developing manufacturing processes which are used to create 3D micro products by layer-layer deposition. EDD is just reverse of EDM process and is achieved by reversing the polarity of tool and workpiece. In EDM tool is connected to negative polarity and workpiece is connected to positive polarity. Fig.1 represents the schematic diagram Electric discharge deposition process. The working principle of Electricdischarge deposition (EDD) is similar to EDMprocess, the only difference is deposition of material in place of machining.

In EDD process similar to EDM, tool and workpiece are come closer to generate a spark. As the applied voltage in discharge gap reached to break down voltage dielectric behaves like conducting medium and current is flowing through it which generate the spark for few microseconds. When sparking take place dielectric fluid is ionized and accelerated towards the electrodes and due to applied reverse polarity electrons are accelerated to a positive polarity (tool). Due to the collision of electrons with toolsurface intense heat is generated at microscopically small region and this tends to melt and vaporization of the tool. The vaporized and melted material from the tool deposited over the substrate-air is used as a dielectric medium to fend off bubble mechanism which generally takes place in EDM process when liquid is used as a dielectric. The temperature at the core of plasma is reached around 8000 to 12000

degree centigrade when spark takes place [23].Due to this temperature, some of the dielectricsis vaporized and formation of bubble takes place to create turbulence in the dielectric tank. As bubble gets collapse turbulence occurs, due to the pressure difference, which is not favorable in case of deposition.

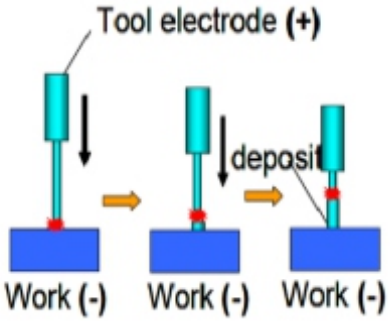

Fig. 1.Schematic diagram of EDD process [11].

II. MATHEMATICAL MODELING AND SIMULATION

THERMAL MODEL

The electrical discharge in the EDM proces is highly complex and uncertain in nature; so, in order to simplify the mathematical model, the following assumptions are formulated:

- The analysis is done for five successive discharges.
- Workpiece and tool are considered to be homogeneous and isotropic.
- Gaussian distribution of heat flux is assumed as heat source [24].
- To model, this periodic heat load is considered as a heat source.
- EDM spark channel is considered as a cylindrical column and the spark radius is assumed to be a function of discharge current and time [8].
- Only a fraction of total spark energy goes to tool and workpiece, the rest energy is lost into dielectric by convection and radiation.
- The properties of electrodes like thermal expansion, density and element structure are not temperature dependent.
- Modeling has been done by considering axisymmetric domain.
- Heat transfers between the electrodes are considered to be through conduction.
- The heat source is supplied for a known time interval.
- A non-linear transient thermal expression is taken into consideration to explain EDD process.

The thermal heat diffusion equation is taken as governing equation.

$$\frac{1}{r}\frac{\partial}{\partial r}\left(or\frac{\partial T}{\partial r}\right)+\frac{\partial}{\partial z}\left(k\frac{\partial T}{\partial z}\right)=\rho C\frac{\partial T}{\partial t} \qquad (1)$$

The initial condition means before the start of the process when tool and workpiece do not come closer. At t = 0, the initial temperature of the electrode is TO (298 ºK) with the surrounding pressure of 101.325 KPa because the electrode is surrounded by air at room temperature as a dielectric medium. The initial condition means before the start of the process when tool and workpiece do not come closer. At t = 0, the initial temperature of the electrode is TO because the electrode is surrounded by air at room temperature as a dielectric medium. The initial temperature (T0) of the tool domain is room temperature which is assumed to be 298 ºK with the surrounding pressure of 1 atm.

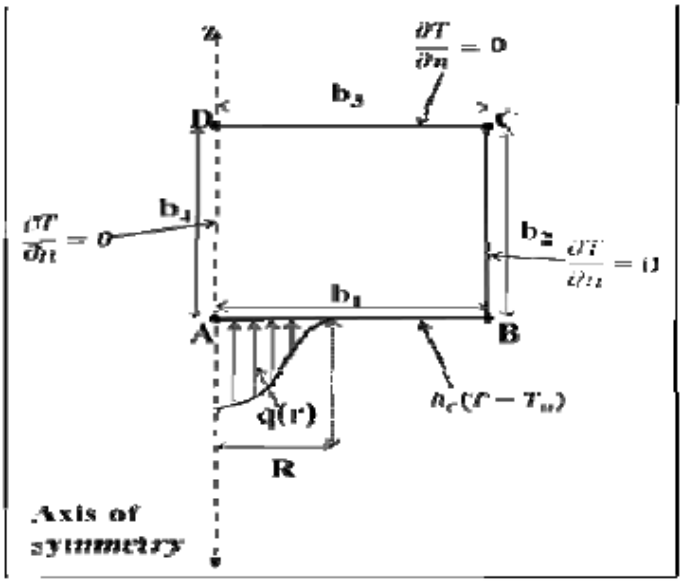

Fig. 2.axisymmetric thermal models for EDD.

The thermal model with boundary conditions shows in the Fig.2.The area ABCD represents the tool which is axisymmetric about the z-axis. The radius of plasma is shown in Fig. 2 where heat flux is applied which is in Gaussian in nature. Electric discharge deposition is carried in a dry medium, i.e. air is dielectric medium.

The conductive boundary b_1 which is in contact with air is modeled. The boundaries b_2, b_3 are assumed to be insulated because the temperature gradient is zero The conductive boundary b_1 which is in contact with and the heat transfer through these boundaries is considered to be zero. The boundary b_4 is the axis of symmetry and also no heat transfer through this boundary. The boundary condition is represented as follows:

At boundary surface b_1

$$\left(k\frac{\delta T}{\delta z}\right) = \begin{cases} q(r) & \text{if } r \le R \\ h_c(T - T_O) & \text{if } r \Sigma R \\ 0 & \text{pulse off time} \end{cases}$$

On boundaries b2, b3 and b4 $\frac{\delta T}{\delta n} = 0$

q(r represents the Gaussian Heat flux applied at anode surface (W/m2), hc represents the convective heat transfer coefficient of dielectric medium (W/m2K), R is the Spark radius (m), T is the ambient temperature (K), TO is Dielectric temperature (K), 'r' represents Coordinate axes, 'n' represents direction normal to the boundary. The radius of plasma depends on operating input parameters. The radius of spark is not measurable due to complexity in spark discharge process and also sparking is occurs for the very short duration, for microseconds. Many researchers proposed a different method to calculate the plasma radius. An empirical expression is pro osed by Erdenet al. [3], the radius of spark is depending on applied current and pulse on time. An anode model is purposed by Patel et al. [18] in 1989 and he told that the spark radius is the product of some constant and time exponent. Also, spark radius is purposed on the basis of boiling point by Panday et al [17].

The equation purposed by Ikai and Hashigushi, [8] is taken into consideration to simulate this model. The expression for the radius(R) is expressed as a function of applied current (I) and pulse on time (Ton). The expression of radius for heat input is given by;

$$R=(2.04 \times e^{-3}) \times (I^{0.43} \times T_{on}^{0.44}) \qquad (2)$$

In this simulation, Gaussian heat is taken in consideration Ikai and Hashigushi, [8] and the expression for heat flux is given byq(r);

$$q(r) = q_o \times \exp\{-4.5 \times (r)^2\} \qquad (3)$$

Where q(r)is the heat flux at radius r (W/m^2),q_o is the Ma imum heat flux at the center of the tool (W/m^2).

In the present simulation, modeling is done for consecutive five discharges. The expression 3.3, we can rewrite in terms of V, I and F_A as follow;

$$q(r) = \frac{4.45 \times F_A \times V \times I}{\pi \times R^2} \times \exp\{-4.5 \times (\quad)^2\} \qquad (4)$$

F_A = Fraction amount of heat input to the copper tool surface, V is the applied discharge voltage (V), I is the applied discharge current (A). To apply periodic heat input, we will introduce an analytic function pulse (x) for duty factor equal to three and Ton equal to 0.75 that uses the Boolean expression: (x<3.75e-7) ||(x>1.875e-6) and multiply pulse(x) with q(r) to generate periodic heat load.

For different duty factor, the expression for the pulse(x) has been changed. The graphical representation of periodic pulse(x) is shown in Fig.3. The amount of heat goes to the tool, workpiece and dielectric are also one of the important factors, which is taken into consideration during modeling. Many researchers considered that equal amount of heat transferred to electrodes. DiBitonto et al.[18] reported that 0.8% of total heat is transferred to the anode. Also, it is reported that 4.8% and 2.2% of total heat energy is

transferred to the anode, by Xia et al. [23] and Yeo et al. [25] respective. In this simulation different values of FA are taken into consideration and analyzed and it is found that 22% establish a goodrelationship between simulated and experimental results.

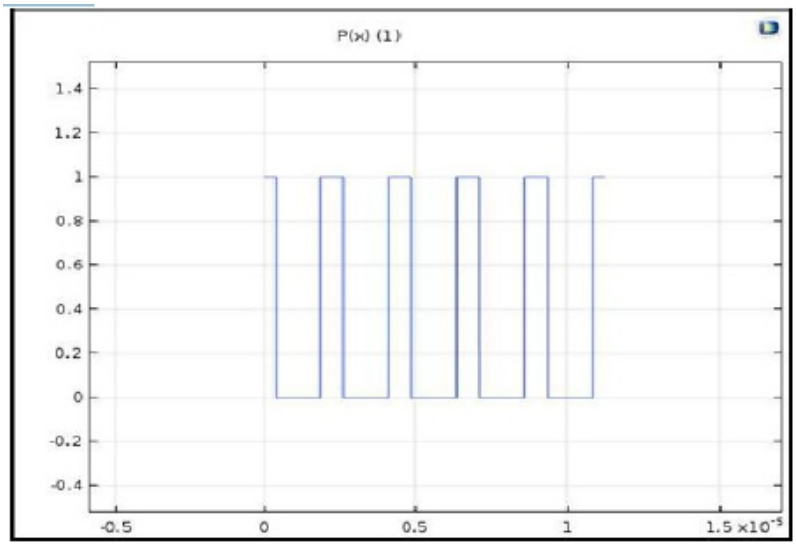

Fig. 3.Pulse function for Ton = 0.75 and t = 3.

DEPOSITION MODEL

The mass deposition model is done to get the height and weight of the deposited material. The volume of deposited material is obtained by thermal model during every single spark. The volume of deposited material is represented as a 3D domain as shown in Fig.4. The 3D domain of deposition model is considered as a hemisphericl cap. Also, the inter- electrode gap is added to the domain with air as a dielectric medium. The melted material is consisting of both liquid and vapor state of metal. Analysis of deposition model is done based on "Theory of heavy species transport by Kee et al. [10], and Patel et al. [18].

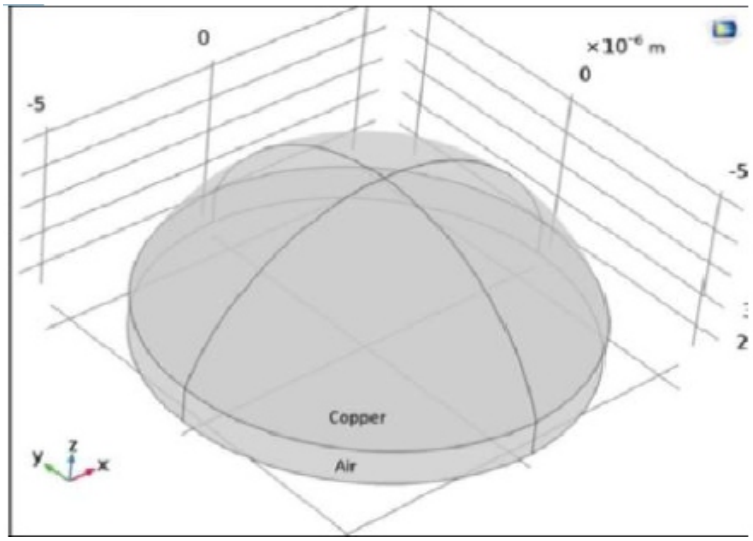

Fig. 4.Domain of the Deposition model

There is a different type of formulations is available for modeling of mass transport phenomenon of a species. The Maxwell-Stefan formulations conserve the total mass in the system along with a few auxiliary constraints by Hagelaar et al. [6].One approximation is to make the diffusive mass transport a function of the gradient of mass fraction rather than mole fraction. The behavior of chemical kinetics controls the plasmas behavior more than diffusive transport. This allows the model to adopt formulations of the Maxwell-Stefan equations. Solution methodology for the deposition model is made by adopting the principles and formulations as per the literature Kee et al. [10].

The multi-component diffusion equation for a flow reaction which has k=1 to Q species and j=1 to N reactions. For the first species, transport of the heavy species (non-electron species) is determined by solving a modified form of the Maxwell-Stefan equations is given by equation (5);

$$\rho \frac{\delta}{\delta x}(w_k)+\rho(u\cdot \nabla)(w_k)=\nabla \cdot j_k+R_k \qquad (5)$$

Where, j_k is the diffusive flux vector, R_k is the rate expression for k^{th} species (kg/m^3s), u is the mass averaged fluid velocity vector (m/s), ρ is the density of the mixture(kg/m^3), wk is mass fraction of the k^{th} species. The diffusive flux vector for the Maxwell- Stefan equation is expressed as in equation (6)

$$j_k=\rho w_k v_k \qquad (6)$$

vk= multi-component diffusion velocity for species k. Multi-component diffusion velocity for a species is defined by equation (7)

$$v_k=\sum_{j=1}^{Q} DK_j d_k - \frac{D_k^T}{\rho w_k}\nabla \ln T \qquad (7)$$

Where DK_jMulti-component Maxwell-Stefan is diffusivities (m^2/s), T is the gas temperature (K), $D_k^T$is the thermal diffusion coefficient (kg/ms), dk is the diffusion driving force (1/m).Eq. The reaction rate of surface species is determined by the Eq. (3.8). The exact amount of melted and vaporized copper material, which is deposited over the substrate, is determined by surface reaction rate. The surface reaction rate for reaction qi is given by equation (8);

$$q_i = k_{f,i}\prod_{k=1}^{K} C_k^{v_{k,i}} \qquad (8)$$

The rate constant, $k_{f,i}$ is given by Eq. (9);

$$K_{f,i} = \frac{(\gamma_i)}{1-\frac{\gamma_i}{2}}\left(\frac{1}{T_{tot}m}\right)\frac{1}{4}\left(\frac{8RT}{GM_n}\right)^{\frac{1}{2}} \qquad (9)$$

ck is the molar concentration of k^{th} species which may be a volumetric or surface species, m is reaction order minus 1, T is surface temperature(K), R is the gas constant, Mn is mean the molecular weight of the gas mixture (kg/mole), γi is the dimensionless sticking coefficient. The surface site concentration for a surface species is determined by solving equation (10);

$$\frac{d\Gamma}{dt} = \sum_{i=1}^{N} q \nabla \sigma_i \qquad (10)$$

Γ is surface the site concentration (mole/m^2), q_i is the reaction rate for ith reaction (mole/m^2), $\nabla \sigma_i$ change in site occupancy number for ith reaction (dimensionless). The surface reaction rates are obtained by solving equation (11), which specifies the site fraction number.

$$\frac{dZ_k}{dt} = \frac{R}{\Gamma_{tot}} \qquad (11)$$

Γ_{tot} is the total surface site concentration (mole/m^2), Z_k is the site fraction (dimensionless), R is the surface rate expression (mole/m2). The height of deposited material over the surface is determined by the equation (12). The following equation is solved for the deposition of height, for bulk surface species,

$$\frac{dh}{dt} = -\frac{RM_w}{q} \qquad (12)$$

Where 'h' is total growth height (μ_m), M_w is molecular weight (kg/mole); ρ is the density of the bulk species (kg/m^3).

III. RESULTS AND DISCUSSION

3.1. THERMAL MODEL

The temperature distribution in the copper electrode is observed during the multi discharge. The main reason for the removal of material is temperature. When the temperature of the electrode reached to melting point temperature, electrode gets melt and deposited over the substrate. In the deposition, the process temperature is the very first parameter; and analyzed for different input parameters. Fig.5 shows the temperature of the copper electrode for five consecutive discharges.

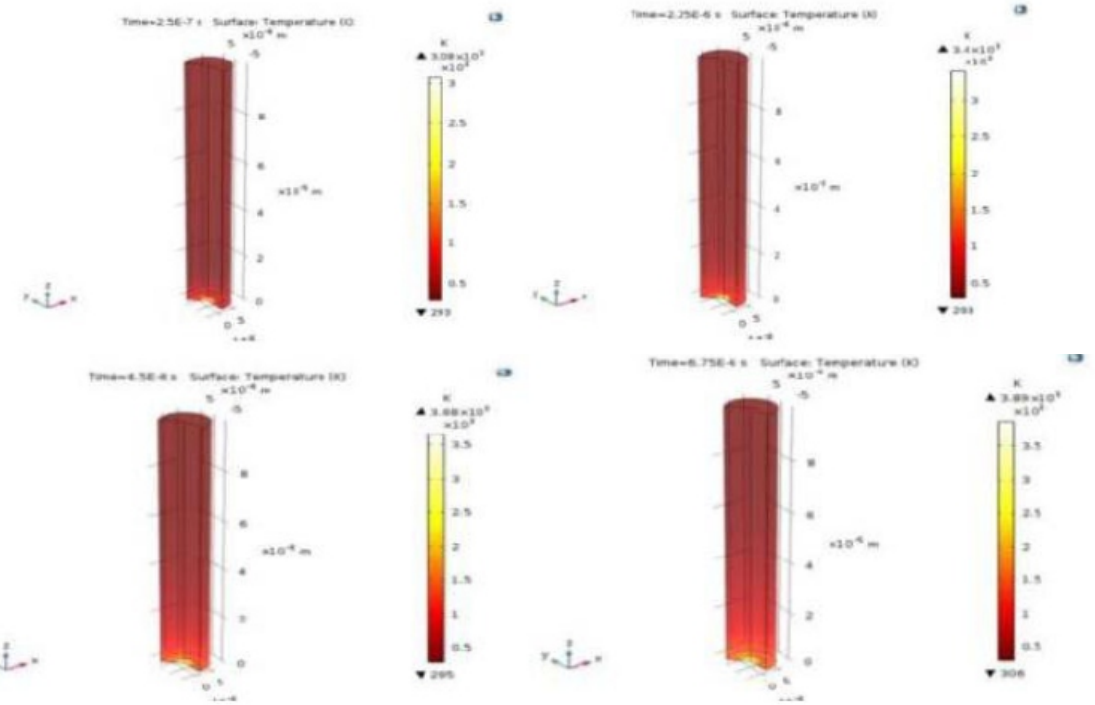

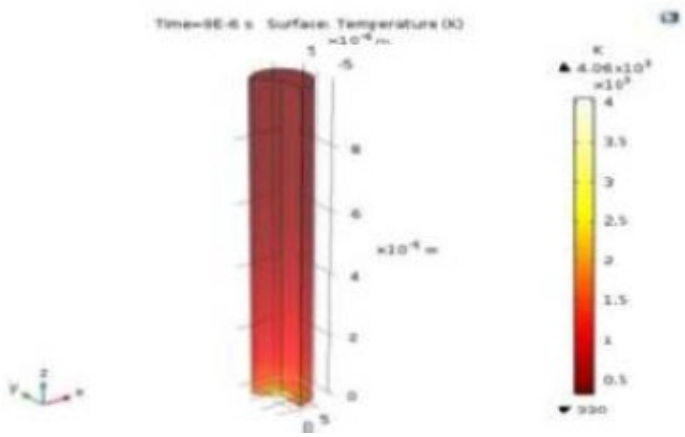

Fig. 5.Temperature distribution in tool electrode for five consecutive discharge.

The value of temperature is more at the center of the electrode and as we move far from the center temperature gets decreased. The temperature within the electrode is increased after each spark because of the residual temperature. The residual temperature comes in the picture due to very less time interval between two consecutive discharges. Due to very less time tool not able to dissipate heat to the ambient.

The melting point of copper 1356 K, thus the is region above the melting point of electrode gets melted. The region which is above the melting point of the copper electrode is shown in the figure by yellow color. Fig.6 shows the variation of temperature for five consecutive discharges with respect to the electrode radius and the Fig.7 shows how residual heat energy increase the temperature of the core of electrode with respect to time and number of spark.

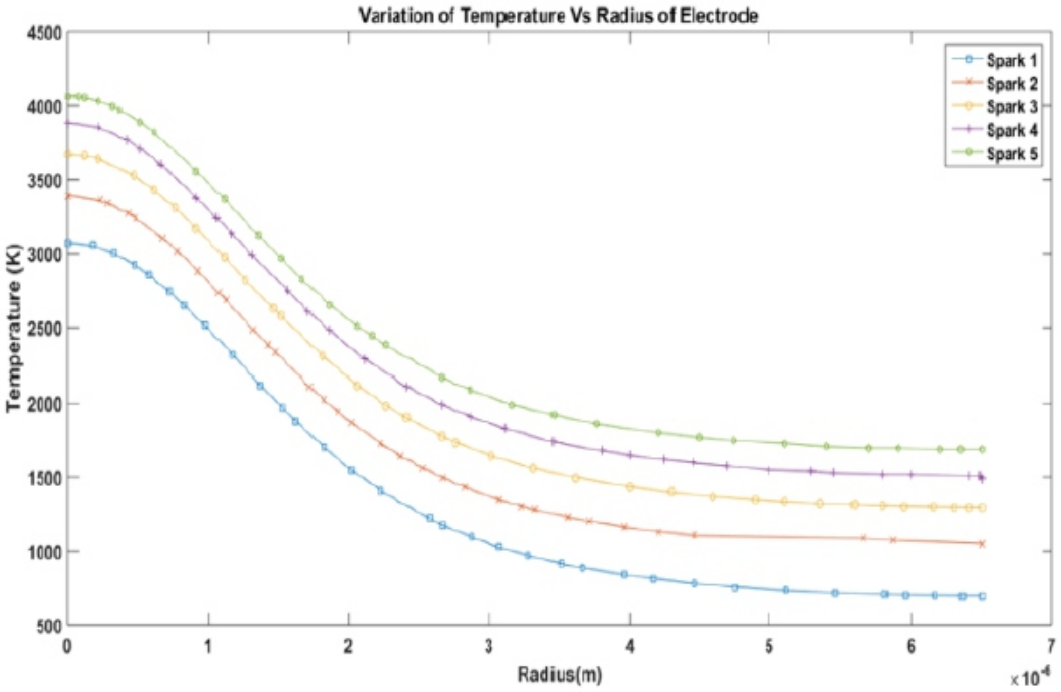

Fig. 6.Variation of the temperature of the electrode with respect to the radius.

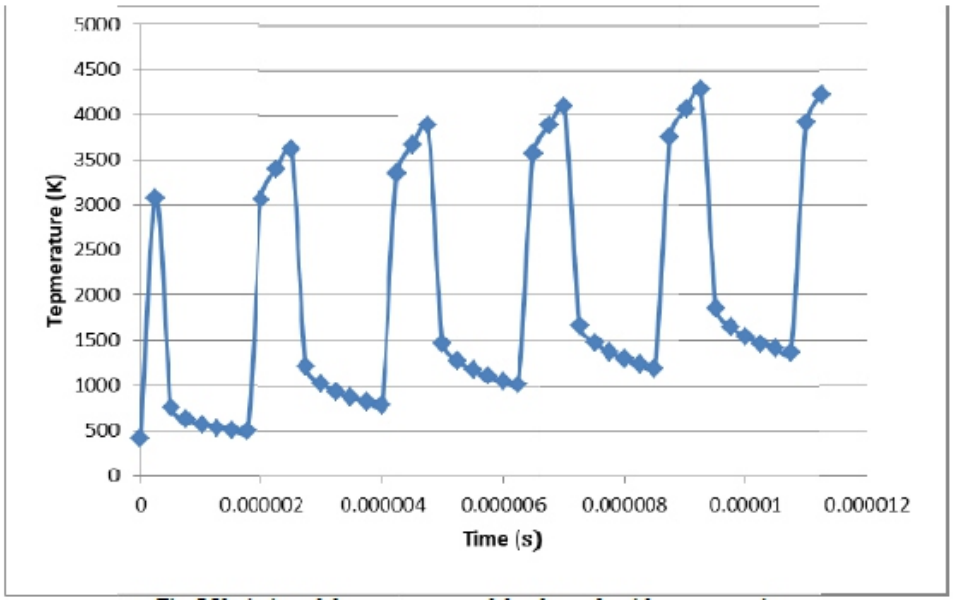

Fig. 7.Variation of the temperature of the electrode with respect to time

3.2 DEPOSITION MODEL

Fig.8 shows the deposition thickness growth after five sparks in parametric extruded view for the input parameter I = 1.5, Ton= 0.75 and t = 3 and V= 60. From figure at the center i.e. the dark red colour shows the maximum deposition thickness, as we moves out ward from the center deposition thickness gets decreased.

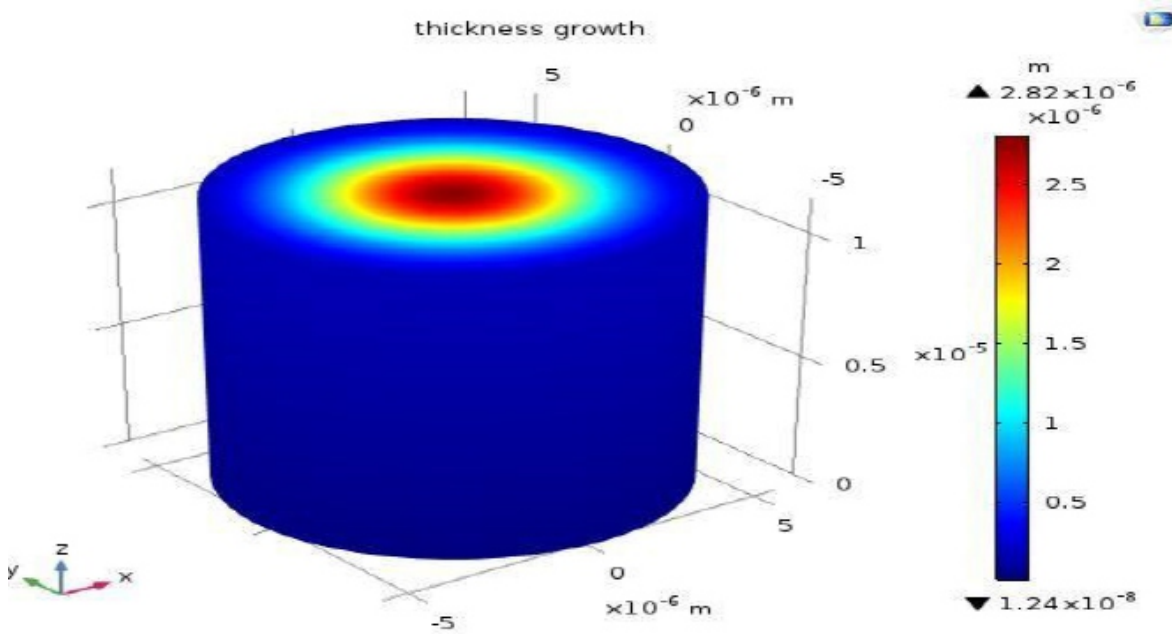

Fig.8. Deposition thickness growth after five sparks.

The Fig.9 shows the variation of deposited material thickness with radius. The Fig.10 shows the parametric extruded view of deposition weight for the five consecutive discharges. In 1st discharge .86ng copper is deposited on the substrate. During 2nd discharge some of the deposited material (1st

discharge) is eroded due to this total deposition of mass after 2nd discharge is not multiple of number of discharge and same phenomenon is happened till the end. The Fig.11 shows the graphical representation of deposited weight with respect to time of spark.

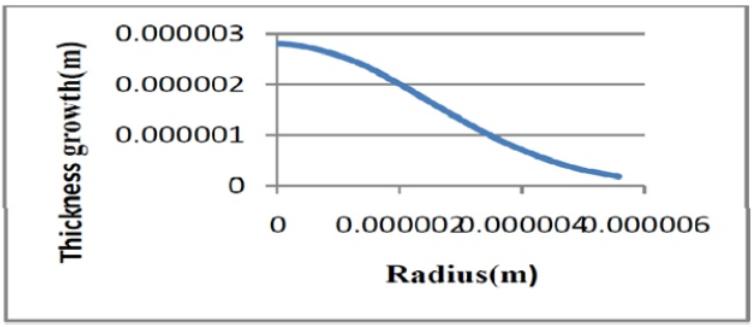

Fig.9. Deposited material thickness with radius.

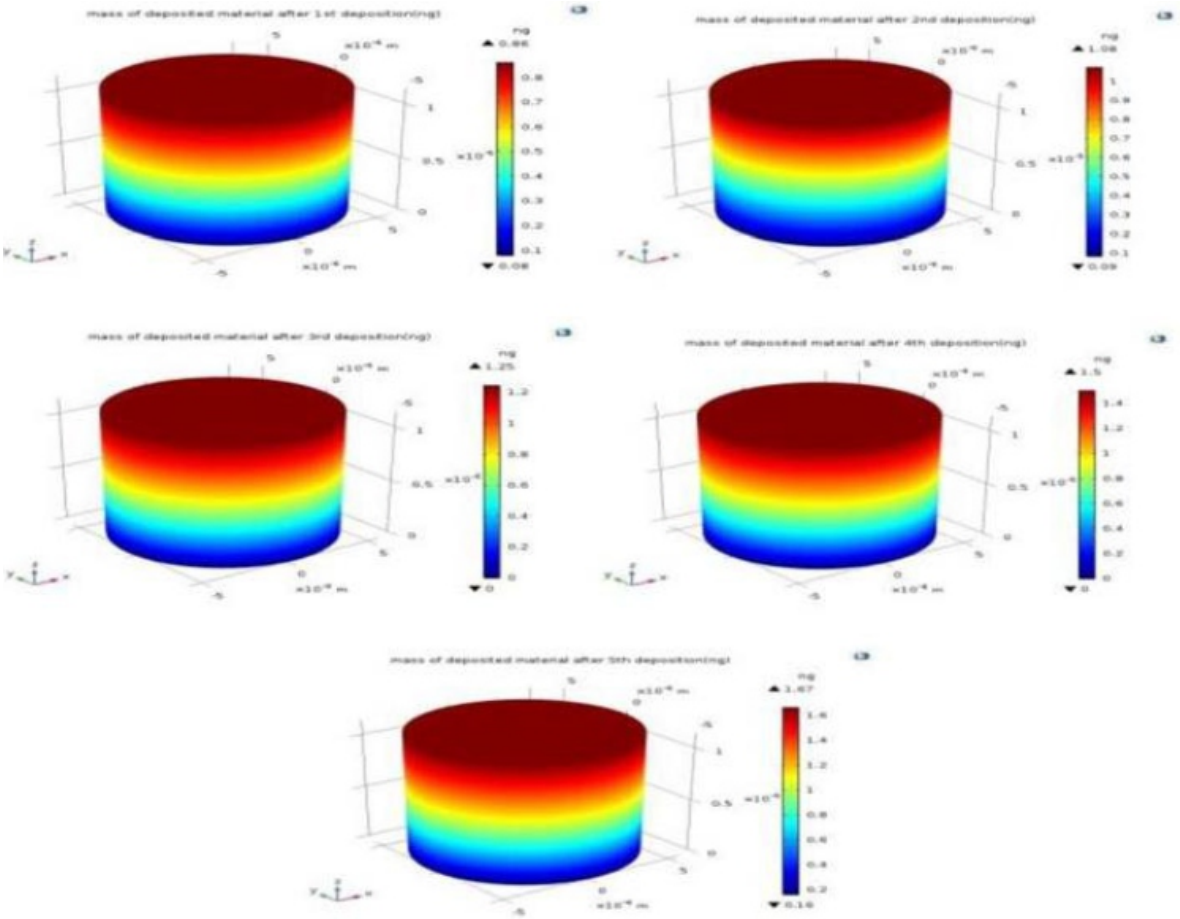

Fig.10. Deposition weight for the five consecutive discharges.

The density of the deposited material (2710 kg/m^3) is much less than the pure copper (8700 kg/m^3) because the deposited material is not a pure copper because during spark copper reacts with O2 present in atmosphere and forms Cu2O.It is observed by Muralidharan et al Error! Reference source not found.that when the air is used as a dielectric medium the chemical composition of deposited layer by weight percentage is, Carbon(C)-46.80%, Copper (Cu)-38.63, Ferrous (Fe)-3.45%, Oxygen(O)-9.8%, Chromium (Cr)-1.12%, because of these composition of deposited material density gets decreased. The Fig.12 shows the density of the deposited material.

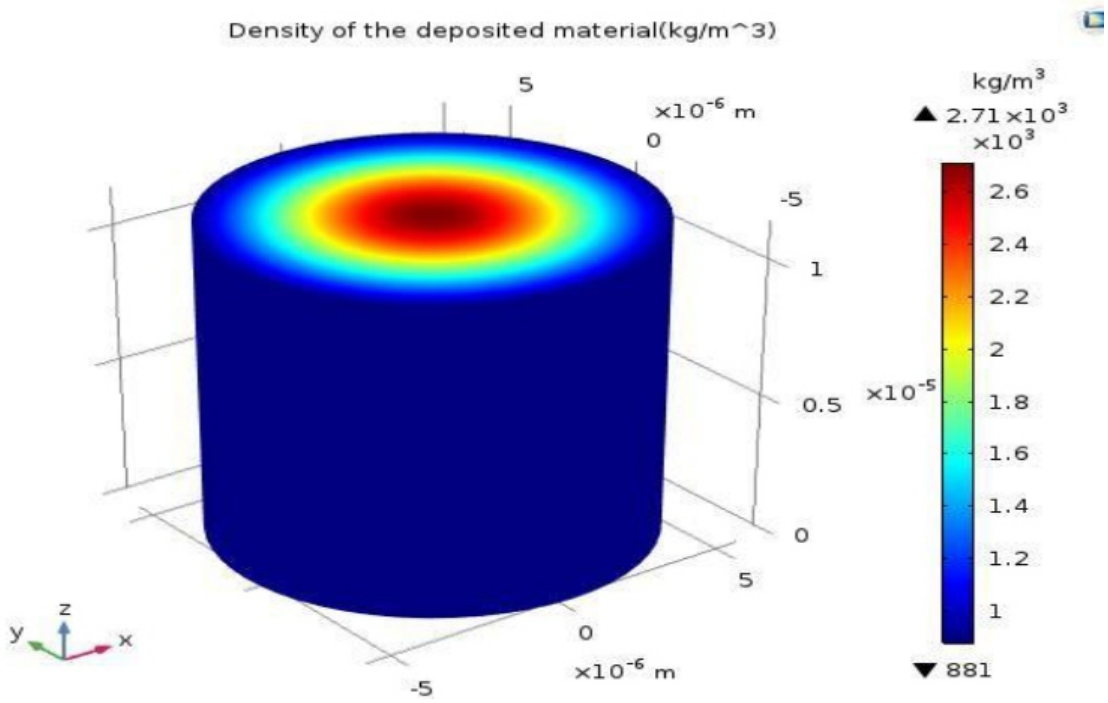

Fig.12. Density of the deposited material.

IV. CONCLUSIONS

This In the present work, the deposition of material through EDM process for multi-spark discharge is modeled and analyzed the height and the weight of the deposited copper material through COMSOL Multiphysics software.

A thermal model has been developed in order to see the volume of melted material removed from the tool. The simulation of the multi-spark discharge deposition process is carried out in presence air as a dielectric. Summarizing, the main features, we draw the following conclusions:

1. A thermo-physical model is developed assuming Gaussian heat distribution and the Heavy species transport phenomenon is applied to understand the deposition process.
2. Experimental values of height and weight can predict using the developed thermo-physical model.
3. The weight of the deposited material is not multiple of number of discharge because during every discharge some material is eroded from the substrate.
4. The density of the deposited material (2710 Kg/m^3) is less than the density of copper because the deposited material is not a pure copper (8700Kg/m^3) because during spark copper reacts with 2 present in atmosphere and forms Cu_2O.

REFERENCES

[1] Brousseau, E. B., Dimov, S. S., & Pham, D. T. (2010). Some recent advances in multi-material micro-and nano- manufacturing. The International Journal of Advanced Manufacturing Technology, 47(1-4), 161-180.

[2] Eidelman, S., &Burcat, A. (1980). Evolution of a detonation wave in a cloud of fuel droplets. I-Influence of igniting explosion. AIAA Journal, 18(9), 1103-1109.

[3] Erden, A. (1983). Effect of materials on the mechanism of electric discharge machining (EDM). Journal of Engineering Materials and Technology, 105(2), 132-138.

[4] Gangadhar, A., Shunmugam, M. S., & Philip, P. K. (1991). Surface modification in electrodischarge processing with a powder compact tool electrode. Wear, 143(1), 45-55..

[5] Govindan, P., Gupta, A., Joshi, S. S., Malshe, A., &Rajurkar, K. P. (2013). Single-spark analysis of removal phenomenon in magnetic field assisted dry EDM. Journal of Materials Processing Technology, 213(7), 1048-1058.

[6] Hagelaar, G. J. M. (2000). Modeling of microdischarges for display technology. Eindhoven: Technische UniversiteitEindhoven.Goto, A. (2001). Development of electrical discharge coating method. 13th Proc. Int. Smp. for Electromaching, Bilbao, 2001.

[7] Hayakawa, S. (2001). Fabrication of microstructure using EDM deposition. Proc. of 13th-ISEM, 783-793.

[8] Ikai, T., &Hashigushi, K. (1995, April). Heat input for crater formation in EDM. In Proceedings of the International Symposium for Electro-Machining-ISEMXI, EPFL (pp. 163- 170).

[9] Kadekar, V., Fang, W., &Liou, F. (2004). Deposition technologies for micromanufacturing: a review. Journal of manufacturing science and engineering, 126(4), 787-795.

[10] Kee, R. J., Coltrin, M. E., &Glarborg, P. (2005). Chemically reacting flow: theory and practice. John Wiley & Sons.

[11] Kunieda, M., Bert Lauwers, K. P. Rajurkar, and B. M. Schumacher. "Advancing EDM through fundamental insight into the process." CIRP Annals-Manufacturing Technology 54, no. 2 (2005): 64-87.

[12] Kunieda, M., Lauwers, B., Rajurkar, K. P., & Schumacher, B. M. (2005). Advancing EDM through fundamental insight into the process. CIRP Annals-Manufacturing Technology, 54(2), 64-87.

[13] Mohri, N., Takezawa, H., Furutani, K., Ito, Y., &Sata, T. (2000). A new process of additive and removal machining by EDM with a thin electrode. CIRP Annals-Manufacturing Technology, 49(1), 123-126.

[14] Mohri, Naotake, Masayuki Suzuki, Masanori Furuya, Nagao Saito, and Akira Kobayashi. "Electrode wear process in electrical discharge machinings." CIRP Annals- Manufacturing Technology 44, no. 1 (1995): 165-168.

[15] Muralidharan, B., &Chelladurai, H. (2015). Experimental analysis of electro-discharge deposition process. The International Journal of Advanced Manufacturing Technology, 76(1-4), 69-82.

[16] Muralidharan, B., Chelladurai, H., &Ramkumar, J. (2013, November). Experimental Investigation on Electro-Discharge Deposition Process. In ASME 2013 International Mechanical Engineering Congress and Exposition (pp. V02AT02A003- V02AT02A003). American Society of Mechanical Engineers.

[17] Pandey, P. C., &Jilani, S. T. (1986). Plasma channel growth and the resolidified layer in EDM. Precision Engineering, 8(2), 104-110.

[18] Patel, M. R., Barrufet, M. A., Eubank, P. T., &DiBitonto, D. D. (1989). Theoretical models of the electrical discharge machining process. II. The anode erosion model. Journal of applied physics, 66(9), 4104-4111.

[19] Sarikavak, Y., &Cogun, C. (2012). Single discharge thermo- electrical modeling of micromachining mechanism in electric discharge machining. Journal of mechanical science and technology, 26(5), 1591-1597.

[20] Simao, J., Lee, H. G., Aspinwall, D. K., Dewes, R. C., &Aspinwall, E. M. (2003). Workpiece surface modification using electrical discharge machining. International Journal of Machine Tools and Manufacture, 43(2), 121-128.

[21] Soni, J. S., &Chakraverti, G. (1996). Experimental investigation on migration of material during EDM of die steel (T215 Cr12). Journal of Materials Processing Technology, 56(1-4), 439-451.

[22] WANG, Y. K., XIE, B. C., WANG, Z. L., & PENG, Z. L. (2011). Micro EDM deposition in air by single discharge thermo simulation. Transactions of Nonferrous Metals Society of China, 21, s450-s455.

[23] Xia, H. (1994). Measurement of energy distribution in continuous EDM process. In Proc. JSPE Autumn Conference (Vol. 269).Ho, K. H., & Newman, S. T. (2003). State of the art electrical discharge machining (EDM), 43, 1287–1300.

[24] Yadav, V., Jain, V. K., & Dixit, P. M. (2002). Thermal stresses due to electrical discharge machining. International Journal of Machine Tools and Manufacture, 42(8), 877-888.

[25] Yeo, S. H., Kurnia, W., & Tan, P. C. (2008). Critical assessment and numerical comparison of electro-thermal models in EDM. Journal of materials processing technology, 203(1-3), 241-251.

[26] Zhenlong, P. Z. C. G. W. (2010). Micro electrical discharge machining deposition in air for fabrication of micro spiral structures. Chinese Journal of Mechanical Engineering, 23(2), 1

Instructions for Authors

Essentials for Publishing in this Journal

1 Submitted articles should not have been previously published or be currently under consideration for publication elsewhere.

2 Conference papers may only be submitted if the paper has been completely re-written (taken to mean more than 50%) and the author has cleared any necessary permission with the copyright owner if it has been previously copyrighted.

3 All our articles are refereed through a double-blind process.

4 All authors must declare they have read and agreed to the content of the submitted article and must sign a declaration correspond to the originality of the article.

Submission Process

All articles for this journal must be submitted using our online submissions system. http://enrichedpub.com/ . Please use the Submit Your Article link in the Author Service area.

Manuscript Guidelines

The instructions to authors about the article preparation for publication in the Manuscripts are submitted online, through the e-Ur (Electronic editing) system, developed by **Enriched Publications Pvt. Ltd**. The article should contain the abstract with keywords, introduction, body, conclusion, references and the summary in English language (without heading and subheading enumeration). The article length should not exceed 16 pages of A4 paper format.

Title

The title should be informative. It is in both Journal's and author's best interest to use terms suitable. For indexing and word search. If there are no such terms in the title, the author is strongly advised to add a subtitle. The title should be given in English as well. The titles precede the abstract and the summary in an appropriate language.

Letterhead Title

The letterhead title is given at a top of each page for easier identification of article copies in an Electronic form in particular. It contains the author's surname and first name initial .article title, journal title and collation (year, volume, and issue, first and last page). The journal and article titles can be given in a shortened form.

Author's Name

Full name(s) of author(s) should be used. It is advisable to give the middle initial. Names are given in their original form.

Contact Details

The postal address or the e-mail address of the author (usually of the first one if there are more Authors) is given in the footnote at the bottom of the first page.

Type of Articles

Classification of articles is a duty of the editorial staff and is of special importance. Referees and the members of the editorial staff, or section editors, can propose a category, but the editor-in-chief has the sole responsibility for their classification. Journal articles are classified as follows:

Scientific articles:

1. Original scientific paper (giving the previously unpublished results of the author's own research based on management methods).
2. Survey paper (giving an original, detailed and critical view of a research problem or an area to which the author has made a contribution visible through his self-citation);
3. Short or preliminary communication (original management paper of full format but of a smaller extent or of a preliminary character);
4. Scientific critique or forum (discussion on a particular scientific topic, based exclusively on management argumentation) and commentaries. Exceptionally, in particular areas, a scientific paper in the Journal can be in a form of a monograph or a critical edition of scientific data (historical, archival, lexicographic, bibliographic, data survey, etc.) which were unknown or hardly accessible for scientific research.

Professional articles:

1. Professional paper (contribution offering experience useful for improvement of professional practice but not necessarily based on scientific methods);
2. Informative contribution (editorial, commentary, etc.);
3. Review (of a book, software, case study, scientific event, etc.)

Language

The article should be in English. The grammar and style of the article should be of good quality. The systematized text should be without abbreviations (except standard ones). All measurements must be in SI units. The sequence of formulae is denoted in Arabic numerals in parentheses on the right-hand side.

Abstract and Summary

An abstract is a concise informative presentation of the article content for fast and accurate Evaluation of its relevance. It is both in the Editorial Office's and the author's best interest for an abstract to contain terms often used for indexing and article search. The abstract describes the purpose of the study and the methods, outlines the findings and state the conclusions. A 100- to 250-Word abstract should be placed between the title and the keywords with the body text to follow. Besides an abstract are advised to have a summary in English, at the end of the article, after the Reference list. The summary should be structured and long up to 1/10 of the article length (it is more extensive than the abstract).

Keywords

Keywords are terms or phrases showing adequately the article content for indexing and search purposes. They should be allocated heaving in mind widely accepted international sources (index, dictionary or thesaurus), such as the Web of Science keyword list for science in general. The higher their usage frequency is the better. Up to 10 keywords immediately follow the abstract and the summary, in respective languages.

Acknowledgements

The name and the number of the project or programmed within which the article was realized is given in a separate note at the bottom of the first page together with the name of the institution which financially supported the project or programmed.

Tables and Illustrations

All the captions should be in the original language as well as in English, together with the texts in illustrations if possible. Tables are typed in the same style as the text and are denoted by numerals at the top. Photographs and drawings, placed appropriately in the text, should be clear, precise and suitable for reproduction. Drawings should be created in Word or Corel.

Citation in the Text

Citation in the text must be uniform. When citing references in the text, use the reference number set in square brackets from the Reference list at the end of the article.

Footnotes

Footnotes are given at the bottom of the page with the text they refer to. They can contain less relevant details, additional explanations or used sources (e.g. scientific material, manuals). They cannot replace the cited literature.
The article should be accompanied with a cover letter with the information about the author(s): surname, middle initial, first name, and citizen personal number, rank, title, e-mail address, and affiliation address, home address including municipality, phone number in the office and at home (or a mobile phone number). The cover letter should state the type of the article and tell which illustrations are original and which are not.

Address of the Editorial Office:

Enriched Publications Pvt. Ltd.
S-9,IInd FLOOR, MLU POCKET,
MANISH ABHINAV PLAZA-II, ABOVE FEDERAL BANK,
PLOT NO-5, SECTOR -5, DWARKA, NEW DELHI, INDIA-110075,
PHONE: - + (91)-(11)-45525005

Note